AN ABSTRACT OF THE THESIS OF

CARLTON EDWARD CROSS for the MASTER OF SCIENCE
(Name) (Degree)

in Electrical and Electronics Engineering presented on May 1, 1969
(Major) (Date)

Title: A SIMULATION STUDY OF DYNAMIC POSTURAL STABILITY IN THE DOG

Redacted for Privacy

Abstract approved: _____
Professor Solon A. Stone

An analog simulation of the postural control system (PCS) of a dog is used to illustrate how modern systems simulation can be applied to a study of complex life systems. Even though many bold assumptions were required to adequately simplify the PCS model, the simulation provided intuitive insight and gave a basis for evaluating performance characteristics seen in live dogs. The data presented suggest that the postural control may be significantly velocity oriented and that the body and muscle dynamics produce only secondary effects on postural stability. The motor control functions of the central nervous system appear to be the major determinants of dynamic postural behavior under the conditions of this study.

A Simulation Study of Dynamic Postural Stability in the Dog

by

Carlton Edward Cross

A THESIS

submitted to

Oregon State University

in partial fulfillment of
the requirements for the
degree of

Master of Science

June 1969

APPROVED:

Redacted for Privacy

Professor of Electrical and Electronics Engineering

in charge of major

Redacted for Privacy

Chairman of Department of Electrical and Electronics Engineering

Redacted for Privacy

Dean of Graduate School

Date thesis is presented May 1, 1969

Typed by Clover Redfern for Carlton Edward Cross

ACKNOWLEDGMENT

Because of the interdisciplinary and judgmental nature of this study, I am unusually grateful for the patient assistance and counsel of Professor Solon A. Stone, Dr. J. M. Brookhart and other members of the research group of the Department of Physiology, University of Oregon Medical School, without whose experience and consideration my work could have been nearly impossible.

This work was supported in part by the Department of Physiology, University of Oregon Medical School, Portland, through Grant NB 04744 of the National Institute of Neurological Diseases and Blindness. Additional support was received from the National Aeronautics and Space Administration through a graduate traineeship granted to the author while attending Oregon State University.

TABLE OF CONTENTS

LIST OF FIGURES

LIST OF TABLES

LIST OF SYMBOLS

Analog Variables

x	m	Table position relative to space
y	m	Dog position relative to space
e	m	Dog position relative to table, $(y-x)$
$\dot{x}$	m/s	Table velocity, dx/dt
$\dot{y}$	m/s	Absolute velocity of dog, dy/dt
$\ddot{y}$	m/s^2	Acceleration of dog, d^2y/dt^2
$\dot{e}$	m/s	Relative velocity of dog, de/dt, $(\dot{y}-\dot{x})$
$\bar{e}$	m	Average error
f_H	N	Horizontal force on body
θ	deg	Joint angle
τ	s	Time
ℓ_s	m	Length of muscle for variable joint angle

Parameters or Constants

α		Forward/reverse force ratio
β		Active/passive force ratio
m	kg	Body mass
a	m	Amplitude of table displacement
h	m	Height, length of leg
r	m	Leg lever arm
d	m	Body lever arm

L	m	Length of muscle for 0.0 deg joint angle
k_t	$(N \cdot m)/deg$	TLMS force coefficient
k_s	N/m	SLMS force coefficient
k_{cf}	N	CFLMS force coefficient
k_{vp}	$(N \cdot s)/m$	VPLMS force coefficient
k_d	$(N \cdot s)/m$	Friction coefficient
ϵ_e	m	Error decision level
ϵ_v	m/s	First relative velocity decision level
ϵ_w	m/s	Second relative velocity decision level
ω	rad/s	Radian frequency

Logical Input Variables

W	Second relative velocity level	$\lvert \dot{y}-\dot{x} \rvert > \epsilon_w$
X	Direction of table motion	$\dot{x} > 0$
V	First relative velocity level	$\lvert \dot{y}-\dot{x} \rvert > \epsilon_v$
S	Direction of relative velocity	$(\dot{y}-\dot{x}) > 0$
E	Error level	$\lvert y-x \rvert > \epsilon_e$
P	Sign of error	$(y-x) > 0$

Logical Output Variables

A	Active force condition	(derived)
F	Force directed forward	(derived)

A SIMULATION STUDY OF DYNAMIC POSTURAL STABILITY IN THE DOG

I. INTRODUCTION

General Perspective

Systems simulation has recently been recognized as a powerful tool having nearly unlimited potential within the life science disciplines. Since life systems are inherently complex, life scientists have, of necessity, been largely concerned with describing isolated elements of a total system rather than the complete system itself. When modern systems simulation techniques are applied to the analysis of a complete life system, simulation becomes a tool which can unify and extend knowledge concerning these systems.

This thesis is intended to be a tutorial example (for both engineers and physiologists) of how systems simulation was employed within an interdisciplinary research project designed to improve knowledge concerning the integrative behavior of the central nervous system (CNS) of dogs. Because CNS functions are expressed in the physical body of the dog, the CNS is being studied somewhat indirectly as an integral part of the postural control system (PCS), which may be observed directly. In the simulation of PCS, the CNS is actually represented as a subsystem. The selection of the PCS to be used in this way was a judgmental decision made independently of the

work described herein.

While the information gained from this simulation is relevent to the specific CNS study mentioned, a further goal has been to illustrate how a general simulation approach may be used in some types of physiological studies. Within the context of this thesis, the problem may be expressed as follows:

> Using the PCS of a dog for an example, demonstrate that simulation can be effective for studying functions of a highly complex physiological system (the CNS), and thus, for improving understanding of the system itself.

Background--The University of Oregon Medical School Experiment

Although the work of devising a computer simulation for the PCS once a model is obtained is within the engineering discipline, the background necessary for constructing a suitable model is available only within the realm of neurophysiology itself. Hence, before proceeding, we will examine the specific physical experiment which motivated this simulation study. This thesis may be considered as only a small part of the much more general physiological study described below.

Studies in neurophysiology have provided a great deal of knowledge concerning nerves and nervous activity, but have never been able to reveal how various components of the nervous system interact to produce coordinated physical activity. Because of this lack of

knowledge, a general study has been started by the University of Oregon Medical School Department of Physiology. This study is designed to improve our insight into the integrative functions of the CNS.

The immediate object of the UOMS study is to gain knowledge and experience which will be needed to begin a general study of the CNS by analyzing the PCS of dogs. The PCS was selected because it affords an excellent example of the CNS operating as a feedback-regulated control system and seems to be well suited to experimentation. Also, the body movement which results from PCS activity may be observed visually.

In the UOMS experiment, controlled and reproducible conditions for study of the PCS are created by training dogs to maintain a posture similar to the stance seen in show dogs, while standing on a moveable table. The command posture is a replicable position which the dogs are trained to maintain while standing on the table. Studies have indicated [1] that the animals are able to hold this posture consistently during experimentation. That is, the range of variation is within acceptable limits for the experimental measurements.

When the dog is on the table in the command posture and the table is moved longitudinally, the posture is disturbed and the animal must make an effort to correct his position. The behavior during this corrective period characterizes the postural control function of the CNS and is the major subject of the present UOMS study.

To give a better understanding of the above physical experiment, several photographs of a dog during experimentation are given in Figure 1. The photographs are enlargements of four frames from a motion picture used to study visually the animal's behavior during table movement [3]. In this case, the supporting table was being moved sinusoidally at a frequency of 1 Hz with a peak-to-peak displacement of 0.1 m. Frames B and D show opposite extremes of the table excursion while frame C shows the table's passing through the center of travel. Frame A shows the command posture while the table was stationary.

The arm which connects to the dog's harness was used to sense the body position during movement. Each foot was placed on a pressure sensitive pad used to record weight distributions and, hence, determine the position of the "center of mass" relative to the table.

Why Simulate?

Since it has been claimed above that simulation can be a valuable aid in projects similar to the UOMS study, it is appropriate that we consider several general reasons why this is true. First, as will be explained later, the PCS is quite similar to less complicated and more familiar non-biological control systems. Hence, knowledge of the classical systems may be linked with various PCS characteristics

Figure 1. Enlarged frames from a motion picture. These pictures are enlargements of individual frames from a motion picture of the dog during experimental study [3]. In all but the first picture, the table was moving sinusoidally at a frequency of 1 Hz and a peak-to-peak displacement of 0.10m.

A. Page 6, top.
Quiet standing in the command posture.

B. Page 6, bottom.
The table has just reached the rear-most position.

C. Page 7, top.
The table is moving forward through the center of travel.

D. Page 7, bottom.
The table has just reached the forward-most position.

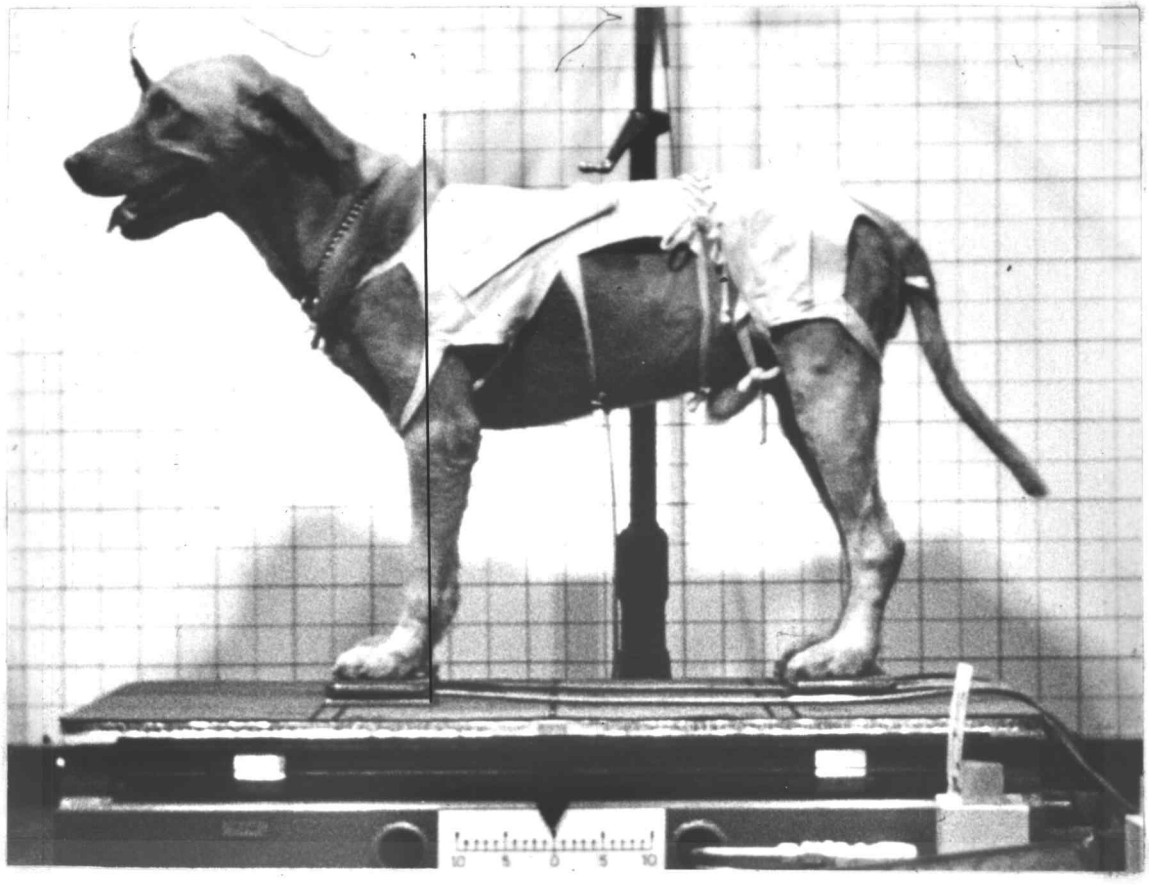

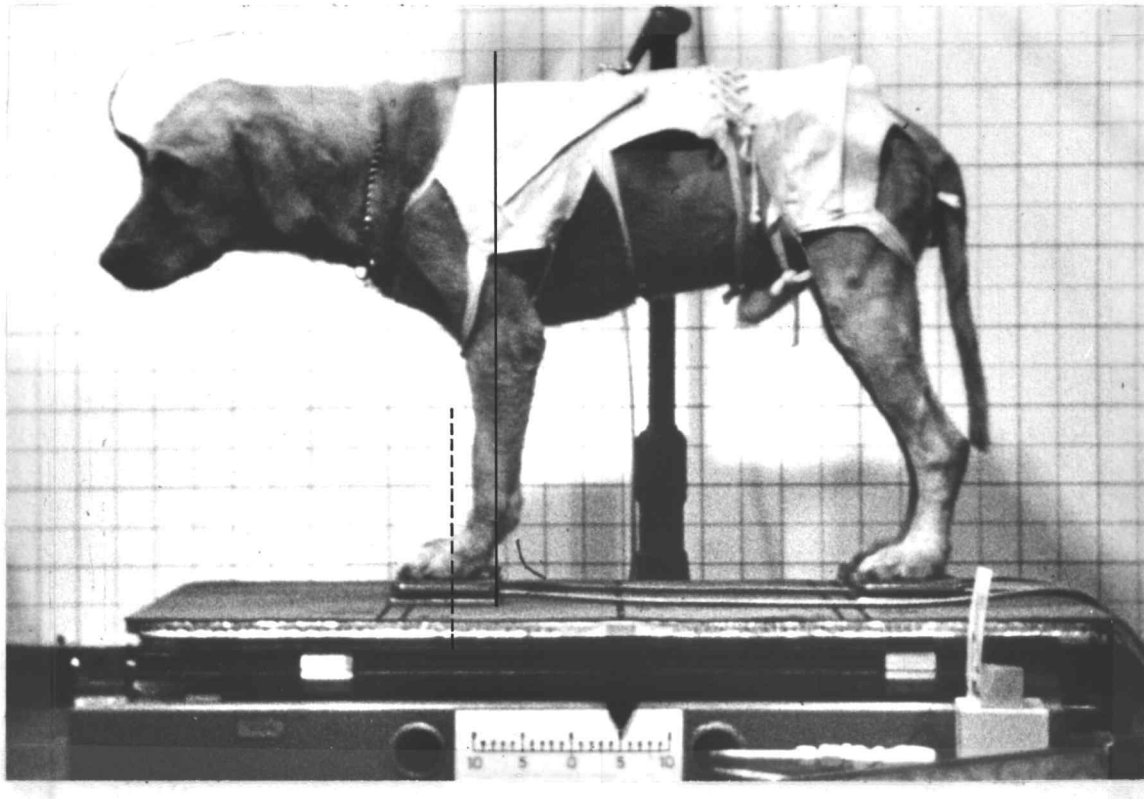

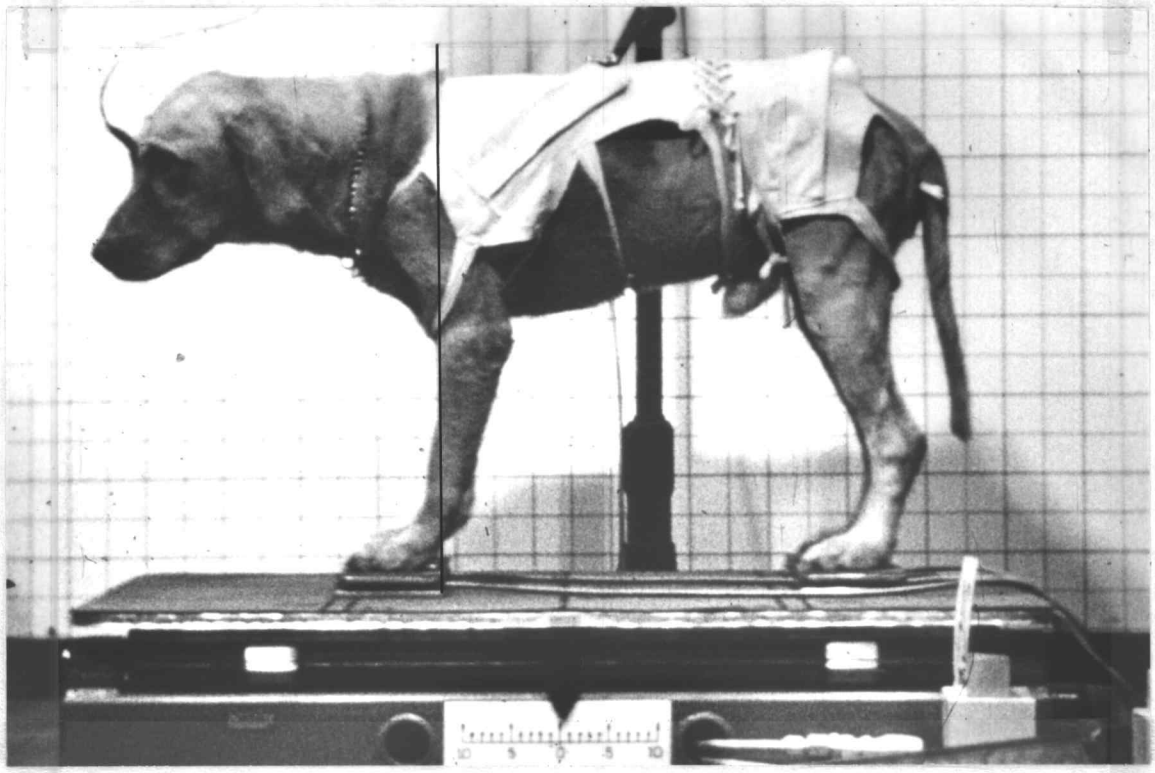

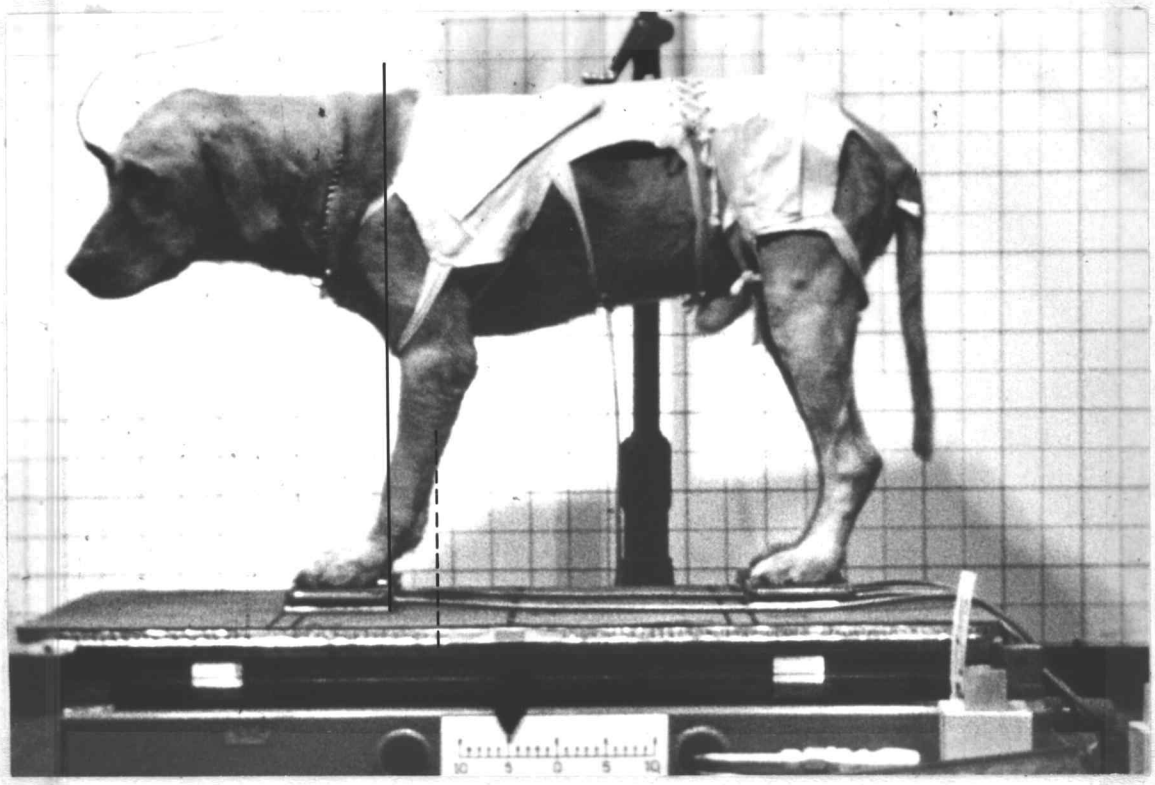

through simulation.

Second, although the CNS is the real point of interest in the UOMS experiment, its function cannot be observed in isolation, but only as it is expressed through the mechanical system of the body mass and legs. Before a serious attempt can be made to understand CNS function, the behavioral characteristics of the mecahnical system must be revealed. Simulation is a well recognized aid for exploring mechanical system characteristics.

Third, the complex nature of the system and its nonlinearities, preclude the opportunity for a theoretical investigation. Since these complications do not negate the effectiveness of computer simulation, simulation remains as a primary alternative to the theoretical approach.

Fourth, simulation is well adapted to the type of simplified, exploratory study which promotes the intuitive insight required for the so called "intuitive leap" which is common to most advances in new areas of scientific study. A major reason for this work has been to gain experience which will strengthen the intuitive understanding needed to plan meaningful experiments with the PCS as the UOMS project continues.

Regarding the latter point, note that a significant question is, "What data should be obtained? " This is critical since the instrumentation required for collecting data from live animals is elaborate.

Hence, one cannot afford to obtain extraneous data where an animal is directly involved, making it very important to have sufficient knowledge to predict the relevance of particular data records before they are obtained. Even a simplified simulation can be useful for finding what data are most relevant.

How Simulation Was Used

The first question to be answered is, "How can one simulate a system such as the PCS, whose complexity far exceeds present knowledge? " In this case, an answer is feasible only because a detailed simulation is not needed for the present. Realizing that the PCS is an elaborate system, the goal has been to deal only with its grosser characteristics as a preparation for more detailed work later. Because of the tremendous versatility of the PCS, the simulation was concerned with the dog in a limited and controlled environment. In general, the approach was to explore several of the basic error-corrective control systems which seemed similar to the PCS and therefore needed to be examined in preparation for an extensive evaluation of the dog's physical behavior during controlled external disturbances.

The different total models used to represent the PCS were all based on a general representation of the system according to the following procedure: First, the dog was represented by the block

diagram of Figure 2A. This was simplified to give Figure 2B. Second, section models of the three major divisions--the CNS, the legs and muscles, and the body--were developed as shown in Figure 3. (Several different section models were formed to represent the muscles and the CNS. Each model contained some feature which might exist in the respective PCS subsystem.) Third, the PCS of the dog was represented by selecting one model for each section and combining the three section models into a complete simulation system. Different characteristics were examined by interchanging one of the section models with an alternate model for that section. Each different combination of the section models gave a distinct representation of the PCS.

To begin this study, a system using very simple section models was chosen and data were obtained for correlating the capabilities of the dog included in the simulation with a set of possible results. These data were then used to develop and modify the section models, thus giving a new system. This method led to an evolution of related PCS models, each representing, to some extent, certain characteristics thought to exist in the dog. Each of these systems is relevant since it may need to be considered in a future study for evaluating the integrative behavior of the CNS while functioning to maintain dynamic postural control (stability).

This thesis discusses the different systems in the approximate

order of their original development. It is felt that the process by which the models evolved may itself increase the intuitive insight of the reader into the general nature of the systems developed and the meaning of the results.

To facilitate examination and description of the above systems, one objective of this work was to produce a catalog of data from each of the systems which were thought to be most representative of the dog's PCS. The data in this catalog were selected to aid in the development of a general intuitive feeling for the types of activity which different PCS models produced. Hopefully, although not complete, these data will provide part of the background information necessary to continue the UOMS experiment efficiently.

While advancing through this paper, we must realize that the nonlinear nature of the systems which were simulated excluded the possibility of a theoretical systems analysis of the models. Further, since there is presently no conclusive way to test the numerous assumptions underlying the simulations, little effort can be made to provide a quantitative analysis of the results. There is a minimal amount of recorded data involving live dogs [3] from the beginning phase of the UOMS experiment which will be used as a guide for evaluating the reasonableness and significance of the simulation results. However, at no time can it be claimed that a particular simulation was correct even if the data obtained agree exactly with existing

records for live dogs.

To meet the general objectives discussed above, the following points will be presented. 1) Following a general description of the complete simulation model, the section models representing the three distinct subsystems of the total PCS model will be discussed separately. These subsystem or section models are known as the body simulator, the leg-muscle simulator (LMS), and the CNS simulator (CNSS). More than one model was used for the LMS and the CNSS. 2) The different simulations of the total system which resulted from different combinations of the section models will be explored in the order they were originally developed, beginning with the most simple. The behavior of each system will be compared with observed behavior in dogs. As the weaknesses of a system become apparent, a modified system will be presented. The behavior of the new simulation system will then be evaluated as before to determine new modifications which should be explored. 3) The data from all systems will be summarized in a catalog form. 4) The final results will be evaluated. 5) Possible conclusions will be discussed.

II. THE MODEL

General Discussion

To begin consideration of an appropriate simulation model for the PCS, we seek first to support the earlier statement that the PCS is an example of a feedback control system. The present hypothesis is that the PCS controls posture according to the following three steps: 1) The present state of the system (body position, velocity, etc.) is evaluated using the sensory inputs to the CNS. 2) This state is compared with an unspecified reference (volitional reference) which is generated in the dog's mind by a training procedure. In the UOMS study, the volitional reference specifies or describes the command posture which the dog seeks to maintain. 3) The CNS generates a physiologically integrated response function to initiate action to correct any errors in body condition which have developed.

Figure 2A shows the PCS in block diagram form. This diagram represents the state of the present hypothesis assumed for the UOMS experiment concerning the PCS. From the diagram, we see that the PCS may indeed by quite similar to more familiar nonbiological control systems.

Figure 2B shows the simplified hypothesis which was used to develop the models presented in this thesis. Note that all but one of the sensory channels were dropped. Initial evidence gathered from

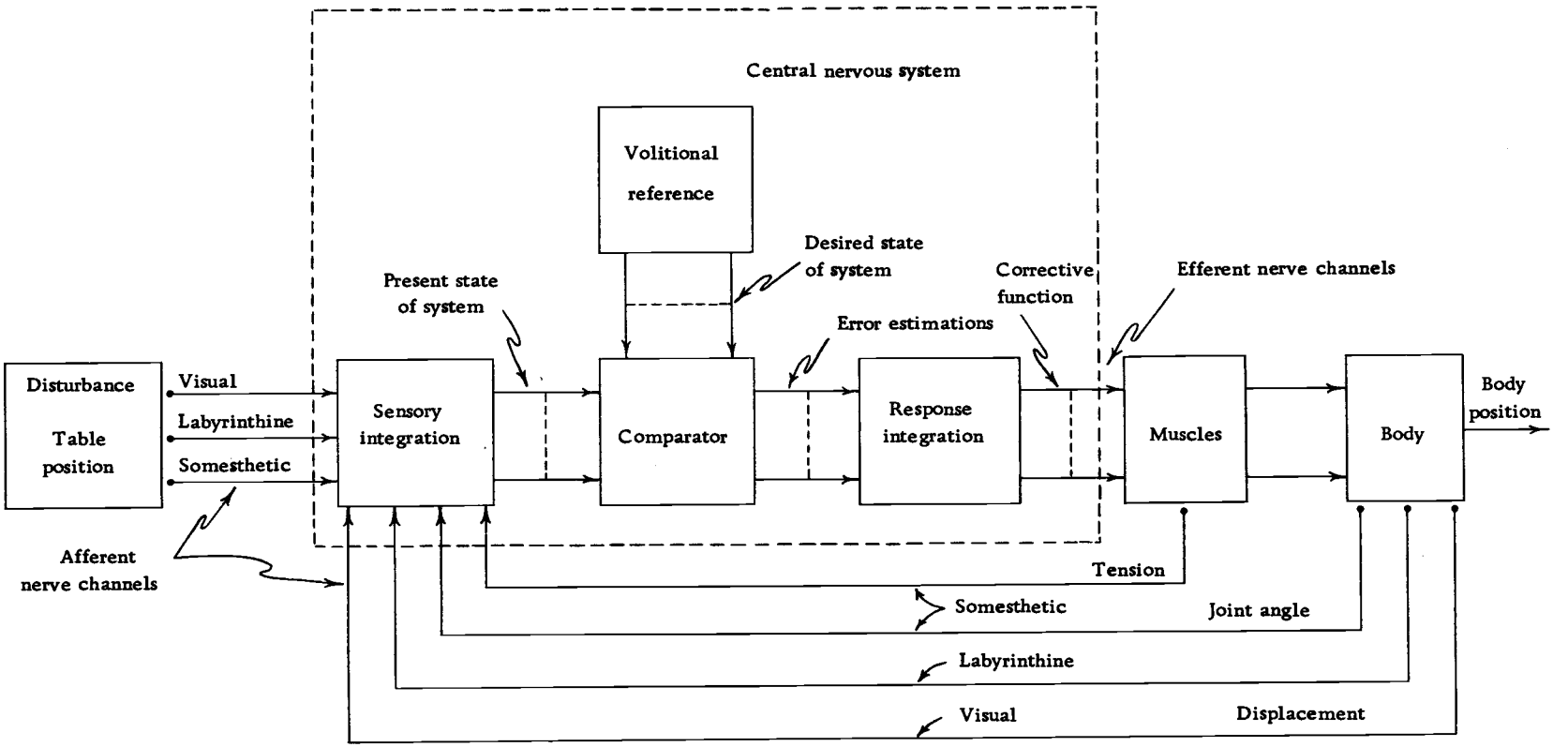

2A. The complete PCS as hypothesized for the UOMS experiment.

Figure 2. Two block diagrams showing how the PCS of a dog is thought to be organized.

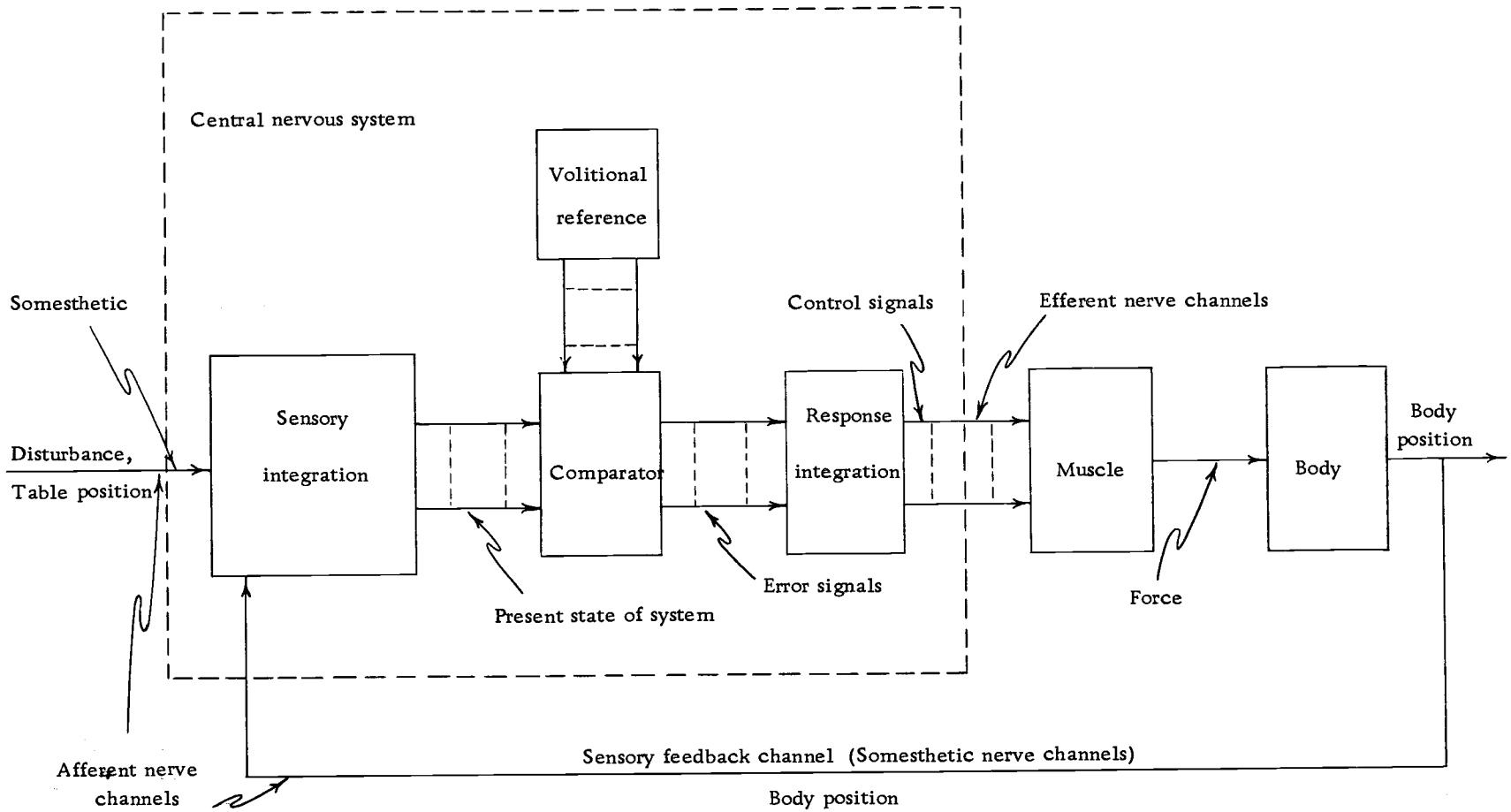

2B. A simplified block diagram used as the basis for this simulation.

the UOMS experiment suggested that the PCS relies importantly on sensory data indicating joint angle [2]. Interrupting other sensory channels caused discernable but not disastrous effects on animal performance [7].

To obtain a simulation model of the PCS under the defined experimental conditions, the dog was first divided into three conceptual sections or subsystems--the body mass, the legs (a set of bony levers activated by the muscles), and the CNS. In the model, the body was represented as a rigid mass which was permitted to move horizontally on the struts formed by the legs. The muscles which activate the legs were controlled by the CNS.

Second, the dynamic behavior of the two mechanical subsystems of the model was described by force equilibrium equations. Also, in this step, the control functions of the CNS were replaced by logical equations which could be implemented using available computer logic. These mathematical equations were then represented on a logic-analog computer where the three subsystems were integrated to obtain the complete simulation based on the general model.

To clarify the second step further, recall that a mechanical mass must obey Newton's laws of force equilibrium. The equilibrium equation which describes the body (subject to forces transmitted through the legs) is a second-order differential equation which was represented by a second order system on the analog computer. The horizontal forcing characteristics of the legs and muscles were

modeled by the LMS, which consisted of a nonlinear force generator designed to approximate one of several possible physical capabilities of the dog. The action of the CNS in controlling the muscles was represented by a simple logic system. The inputs to this simulator (the CNSS) were logic variables defining the state of the body, and the outputs were logic variables which controlled the direction and magnitude scaling of the horizontal force generated by the LMS. Figure 3 gives a block diagram of the resulting computer model of the PCS. This diagram is further explained in the following sections.

It should be added here that the section models of the three subsystems--the body mass, the leg-muscle mechanics, and the CNS--should not be confused with the total simulation system which combines all three of these. The total system will be designated by first identifying the CNSS being used and next stating which LMS is representing the leg-muscle mechanism. As an example, the first system considered was CNSS 0; TLMS. The CNSS is specified first since the logic control of the muscles was the most distinguishing characteristic of each of the complete systems. The body simulator used the same model throughout and therefore was not specified.

The Body

The first step in developing an adequate simulation model of the PCS was to assume a reasonable mechanical model to represent

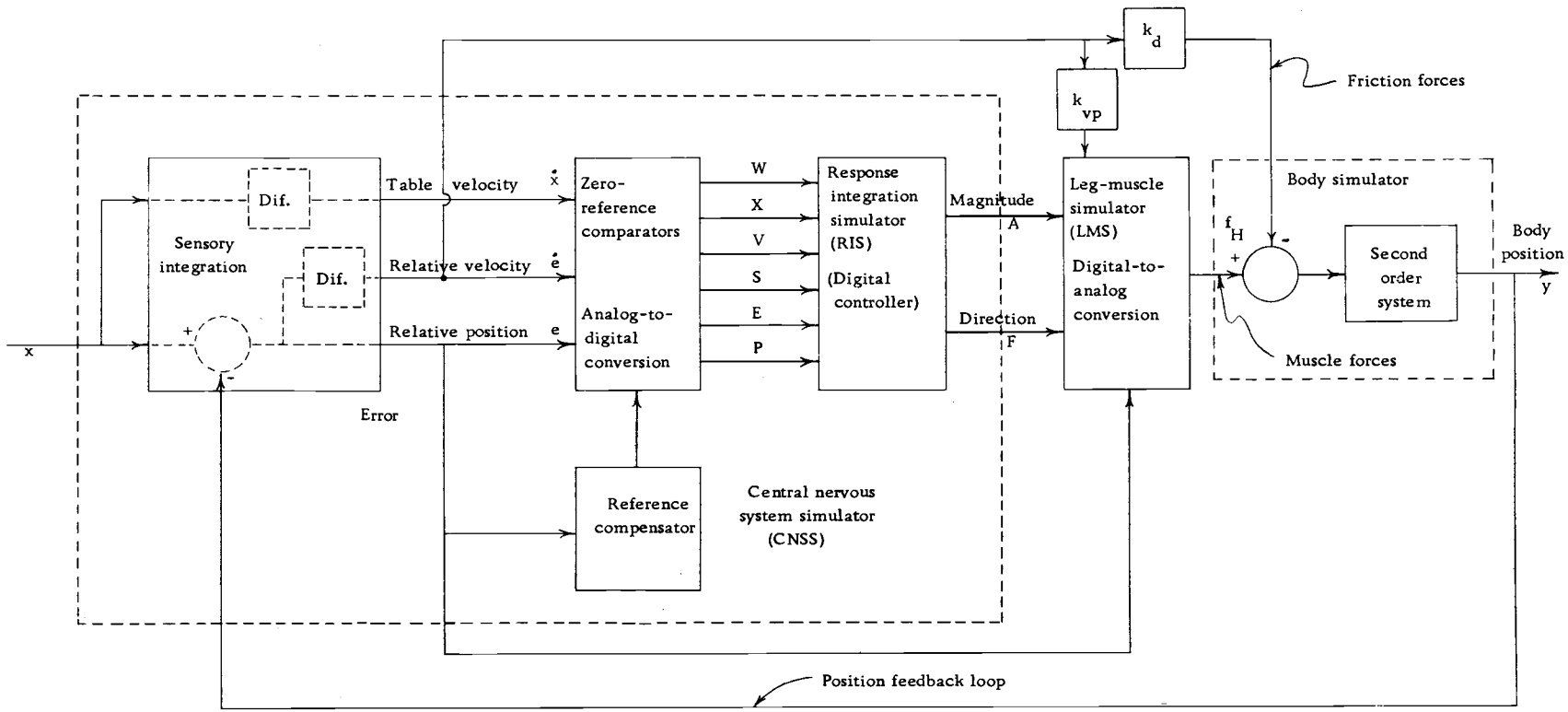

Figure 3. A block diagram showing how Figure 2B was represented on the logic-analog computer. The assumptions required to proceed from Figure 2B to this diagram are discussed in Chapter II. The reference compensator indicated was used for investigations with all systems but was not part of the basic model. The scaled relative velocity input to the LMS was used only for the velocity-proportional LMS (VPLMS) described later. Otherwise, the block should be removed, i.e., $k_{vp} = 0.0$ N·s/m.

the dog's skeleton and mass. From the simplified mechanical model, an electronic analog computer simulation was easily obtained. The mechanical model was based on several major assumptions and simplifications discussed in the following.

It was first suggested that the legs and backbone were rigid members and that the entire body could be treated as a mechanically rigid mass. It was next assumed that the effects of vertical movements of the body mass were insignificant. Since the major portion of mass in the legs was near the body, we assumed that the legs could be considered as massless members if their equivalent mass was included in the body. Because only horizontal motion was to be studied, the head and neck were also included in the body. By postulating that the body was rigid and by neglecting vertical motion, a center of mass was defined midway between the anterior and posterior legs for modeling purposes. Basically, what was done was to make the necessary assumptions for reducing the body to an equivalent point mass.

The model created by the preceding development is shown in Figure 4. Despite the appearance of an unreasonable simplification, the number of variations which might be desired and the indefiniteness of their importance suggested that to deviate appreciably from this simple model would only confuse interpretation of the results of the simulation for the present.

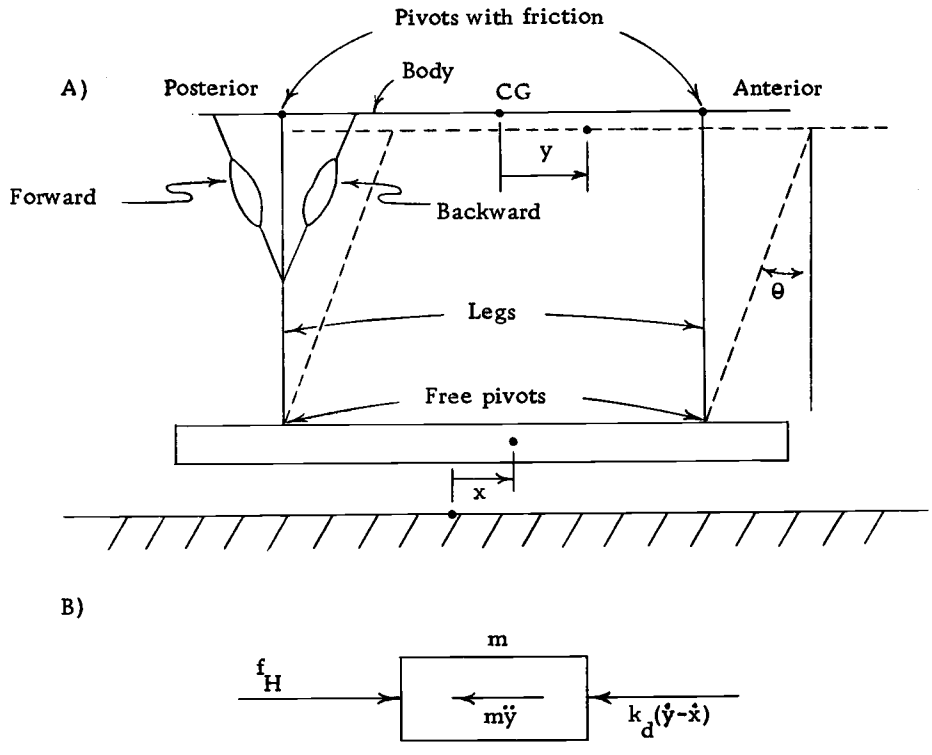

Figure 4. A) A mechanical model to represent the body and leg-muscle structure of the dog. Viscous friction was assumed at the joints. The muscles act in tension alternately according to logic command from the CNSS. B) The force equilibrium diagram.

The equation of dynamic equilibrium for the model is

$$m\ddot{y} + k_d(\dot{y}-\dot{x}) - f_H = 0, \qquad (1)$$

where m is the body mass, y is the position of the center of mass, x is the table position, k_d is the coefficient of viscous friction, and f_H is the horizontal force applied to the body through

the legs. (See the List of Variables for further definitions.) The viscous friction was assumed to originate in the joints and muscles of the legs. It is not known whether viscous friction is an adequate approximation to the real case. Presently, the only existing information regarding friction is for joints [4]. The nature of muscle friction is undetermined, and indeed, may tend to remain so. Hence, the friction coefficient was varied throughout the work to determine the possible effects of a large error on this point.

The Legs and Muscles

In the dog, all forces acting on the body (f_H) were transmitted from the table through the legs. Both the stiffness (tension of the muscles) of the legs and their position (joint angle) determined the magnitude of the maximum force which could be transmitted and was a function of the total muscle activity at any given time. Since the muscle activity in the dog was directly controlled by the CNS, the leg-muscle model needed was simply a force generator whose output could be varied according to the error ($y - x = e$, $\theta \doteq e/h$) and the CNSS output (control) variables.

Because the body model was reduced to a point mass moving only horizontally, the model for the leg-muscle subsystem required only one conceptual leg to represent the four hypothetically identical legs which coupled horizontal forces between the body and the table.

Hence, the basic force generator within the LMS generated only one output as a function of the error to represent the force applied to the body. The functional form of the output for this force generator was determined by the characteristics of the muscle being simulated. The direction and scaling of this basic force function after being generated were controlled by the CNSS output variables A and F (see Figure 3), which will be identified completely later.

The LMS was constructed so that the direction in which the above force was applied could be controlled by the CNSS output variable F. Also, either of two magnitude scaling factors could be selected according to the condition of the CNSS output variable A. Although several different basic force generators were used to represent various muscle characteristics, the logic control variables were always employed in the same way as is described above and more fully in Appendix A. (The magnitude scaling, logic control, and function generation of the LMS are detailed in Appendix A.)

Several broad assumptions regarding the interaction of the motor nerves and the muscles they controlled are implicit in this model. These assumptions were equivalent with the claim that the force response of the muscles was instantaneous upon nerve command. A similar statement is that the muscles operated as an open-loop system (no feedback) with no time delay. (The input would be nerve commands or stimuli and the output would be the desired

tension or force.)

Since the force characteristics of the legs are not known, several different force generators were used in the LMS. The most simple was the torsional generator where the torque applied to the leg was proportional to the joint angle θ. This model assumed that the effort to correct the body position increased linearly as the error increased.

The second generator assumed that the muscle depicted in Figure 4 acted as a linear spring. This again implied that the effort to regain a zero joint angle increased as the joint angle increased. However, the corrective force was not linear with joint angle in this case. The horizontal corrective force which was applied to the body to correct position fell off from the linear case as the joint angle increased.

The third generator to consider rested on the assumption that the muscles were capable of producing the same contractive force upon CNS command for any reasonable joint angle. This simulator assumed that the muscle shown in Figure 4 was a constant-force generator regardless of leg position (joint angle). Thus, the horizontal force decreased only slightly as the joint angle increased.

Finally, the muscle was assumed to produce a force proportional to the magnitude of the relative velocity. Hence, for a constant relative velocity, the horizontal force generated was the same form

as for the above simulator except for the magnitude scaling. This generator was used with only one of the CNSS models.

The LMS's derived from these four models were known as the torsional LMS (TLMS), the spring LMS (SLMS), the constant-force LMS (CFLMS), and the velocity-proportional LMS (VPLMS), each named after the characteristics of the muscle represented by the simulator. The equation for the horizontal force f_H which was produced by each simulator is developed in Appendix A and is presented below. These equations correlate directly with the curves given in Figure 5,

$$\text{TLMS} \qquad f_H = k_t|y - x|/h^2 \quad \text{(A and F, "true")} \tag{2}$$

$$\text{SLMS} \qquad f_H = rdk_s\Delta\ell/(h\ell_s) \quad \text{"} \tag{3}$$

$$\text{CFLMS} \qquad f_H = rdk_{cf}/(h\ell_s) \quad \text{"} \tag{4}$$

$$\text{VPLMS} \qquad f_H = rdk_{vp}|\dot{y} - \dot{x}|/(h\ell_s) \quad \text{"} \tag{5}$$

$$\ell_s = (L + \Delta\ell)$$

which are copies of plots taken from an X-Y plotter. In each of the first three simulators, the appropriate force coefficient-- k_t, k_s, or k_{cf}-- was selected so that the force for a joint angle of 5 deg was 6N when the logic variable A was "true" (active mode). The VPLMS force coefficient k_{vp} was selected so that the generated force was 6N for a joint angle of 5 deg and a relative velocity of 0. 097 m/s.

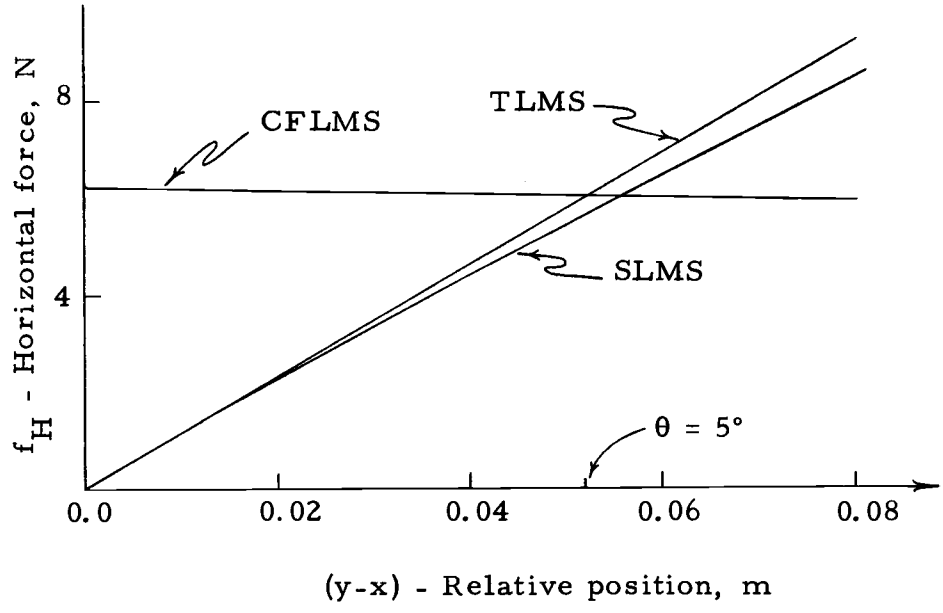

Figure 5. Horizontal force curves for three of the LMS's. These plots, copied from an X-Y plotter, show the force generated when the LMS was in the active mode (A "true"). The VPLMS is not shown since the force magnitude was a function of relative velocity as well as joint angle.

The Central Nervous System

Attention now turns to the CNS which is the central and most elaborate subsystem of the PCS. Modeling of the CNS is inhibited by a lack of intuition regarding how logical processes are actually carried out in the brain [6]. For this simulation, the UOMS hypothesis was used as the beginning point for model development. The block diagram in Figure 2A was essentially the result of the hypothesis and was the first step toward a suitable simulation model of the CNS. A justification of the hypothesis and the resulting CNS configuration is not included in this thesis since both resulted from physiological

rather than engineering considerations. It should be clear, however, that the CNS diagram of Figure 2A follows directly from the hypothesis statement at the first of this chapter (p. 13).

Having accepted the CNS block diagram in Figure 2A, the second step toward a computer simulation was to simplify the diagram so that a computer model could be defined in a way that allowed computer operations to be substituted for the functional divisions of the CNS model. The assumptions employed to gain this simplification are correlated with each block of the diagram below.

The first block is entitled, "sensory integration." This block represents all functions which contribute to a continual evaluation of the posture and follows intuitively from part 1 of the hypothesis. In the dog, this process very likely involves a considerable amount of nonessential sensory data received via the afferent nerve channels. To simulate this block, the posture was evaluated in a way simple enough for easy simulation. For the given model of the body, a convenient simplifying choice was to evaluate the state of the system (body posture) using only the joint angle θ and the rate-of-change of joint angle $\dot{\theta}$ as state variables. By selecting θ and $\dot{\theta}$ it was claimed that for control purposes, the state of the system (the dog on the table) was adequately described by these two variables. Certain data from the UOMS work indicate that joint angle is at least

a dominant control variable. First, a study of quiet standing suggested that joint angle was quite significant for posture control [2]. Second, visual and labyrinthine (body acceleration) sensory data were not required for satisfactory control after an adjustment period [7]. The assumption is simply to class these factors as secondary and neglect them during the study.

Clearly, the selection of θ and $\dot{\theta}$ gave a unique description of posture at any time using a minimal representation of the system. As explained below, this selection is implied by the block diagram of the CNS given in Figure 2B where the only feedback channel is for body position.

More explicitly, the function of the simplified sensory integration block was to evaluate the body position relative to the table position, thus obtaining the relative position or error to be used as a state variable. (Since $\sin \theta = e/h$ and for small error $\theta \doteq \sin \theta$, the joint angle and relative position may be used interchangeably assuming that the proper scale factors are included.) Next, the model required that the error be time differentiated to obtain the relative velocity $\dot{e}$ as a second state variable. This implied that the sensory integration section of the CNS must either be capable of this operation directly or that it actually received the body and table velocities as sensory input data. Distinguishing between these two possibilities does not affect the model which results. In fact,

although the CNS models in Figures 2B and 3 assumed that explicit differentiation was implemented, the computer simulation actually obtained the relative velocity implicitly by comparing table velocity $\dot{x}$ with body velocity $\dot{y}$ to obtain $\dot{y} - \dot{x} = \dot{e}$, since $\dot{y}$ and $\dot{x}$ were directly available from the body simulator and input generator, respectively. The differences between these two views of sensory integration carry physiological significance which, as yet, is undetermined.

After initial investigations of systems based on the above sensory integration model, a modification was implemented in an attempt to include a quite strong predictive capability in the CNSS for periodic table movement. In addition to the two state variables, the table velocity $\dot{x}$ was included as a sensory integration output.

The second block operation indicated required a comparison of either the two state variables alone or the state variables and the table velocity with some reference levels which were obtained from the volitional reference. Hence, the volitional reference simply generated analog reference signals for each system variable. Realizing that the volitional reference is perhaps the most abstract implication of the UOMS hypothesis, it was necessarily modeled with the aid of a very strong assumption, namely that the reference levels were fixed at zero for all variables. This means that the dog was assumed to use an exact, time-invariant reference for all sensory variables. In

truth, the volitional reference is very likely non-constant or stochastic and highly dependent on subjective factors which are relatively unknown. The reference compensator seen in Figure 3 was included in an attempt to study the effects of certain variations in the volitional reference which might occur in the dog.

After obtaining analog variables to describe the condition of the body on the table and the reference position, the next step was to derive error signals by comparing the sensory integration output variables with the volitional reference levels. This gave a set of error variables which were the basis of the corrective control represented by the response integration block, which included the coordinative or integrative capability of the brain and reflex centers external to the brain but within the CNS. Anticipating the logical nature of the response integration simulator (RIS), the analog error variables were coded with a limited number of Boolean logic variables which were inputs to the RIS.

In the last CNSS block, the RIS (Figure 3), logical functions for controlling the LMS were developed to represent the functions of the response integration block (Figure 2B). These logical functions which are described later were intuitively determined in an effort to model the action which the dog seemed able to produce. Realizing that there is no real justification for assuming that the brain functions analogously as modern computer logic [6], the acceptance of this

model should be recognized as simply a pragmatic approach to a complex problem.

The above series of assumptions has led us to the CNS model which was implemented on a computer for this simulation. To summarize, the first assumption to use only three variables-- e, $\dot{e}$ and $\dot{x}$ --to describe the condition of the body allowed a simplification from Figure 2A to Figure 2B. Considering Figure 2B, the volitional reference was set at zero for all variables and the response integration was described by logical functions of the logical error variables. These assumptions gave a model in which computer operations were readily substituted for each of the functional blocks.

Regarding the above substitution, the output variables of the sensory integration block were all derived with analog summers from variables available in the system. These variables (e, $\dot{e}$ and $\dot{x}$) were compared with the volitional reference and logically coded in one step using analog-to-digital comparators. The response integration functions A and F were generated from these logic variables with the customary logical gates. These Boolean functions were used to operate switches in the LMS, thus achieving a digital-to-analog conversion. This is the final simulation model of the CNS as implemented on the computer and diagrammed in Figure 3.

Realizing that the RIS likely represents the most distinctive and central functions of the CNS within the PCS, it was expected that

several different representations of the response integration would be developed in the simulation study because no one representation could be really adequate. Since the RIS was simply a configuration of computer logic used to represent appropriate logic functions, changes from one RIS model to another were readily implemented after the desired logical functions had been determined. These changes were generally accomplished without changing any other part of the CNS model, hence, the particular CNSS being used was a combination of the fixed parts of the model and some particular RIS. To identify the logic systems used, the RIS's were numbered 0 through 3. Clearly, CNSS 2 was the CNSS which used RIS 2.

Before describing the different RIS's by number, the logical variables used as RIS inputs must be defined. The variables E and P were assigned to e and W, V and S were assigned to $\dot{e}$ as follows: E was "true" when $|e| > \epsilon_e$, P was "true" when $e > 0$, W was "true" when $|\dot{e}| > \epsilon_w$, V was "true" when $|\dot{e}| > \epsilon_v$, and S was "true" when $\dot{e} > 0$. The variable X was assigned to $\dot{x}$ with X "true" for $\dot{x} > 0$.

Referring to Figure 9, it is now possible to verify that a given combination of truth values for the RIS input variables denotes a unique region of the phase plane. (The number code in Figure 9 is explained below.) The function of the RIS was simply to assign certain truth values of the output variables A and F to each possible

combination of truth values of the input variables, where a given input combination indicated that the state point was within a corresponding region of the phase plane. Since $\dot{x}$ is not a state variable and does not appear on the phase plane, the addition of X is a special case and will be explained later.

To simplify the above, the same result could have been obtained by dividing the phase plane into 16 different regions. Then, using four logical variables, a unique combination of truth values for the variables could have been assigned to each of the 16 regions as shown in Figure 9, these assignments being the same as were used for RIS 2. With a system of computer logic elements (the RIS), the two variables A and F would then be derived, having truth values that had been assigned to correspond with the particular combination of the input truth values. The net result would have been that the RIS was a means for assigning one of four possible combinations of truth values for A and F to each region of the phase plane, thus achieving a particular control pattern.

Clearly, the characteristics of the separate RIS's were determined by the truth values of the variables A and F which were assigned to a given phase plane region. These assignments were specified for each RIS system with a truth table such as Table 3 on the basis of an intuitive consideration of how the LMS should be controlled to achieve a particular result from the simulation. In the

following development, a truth table and the associated intuitive explanation will be given for each RIS used in the study. The Boolean logic functions A and F are derived for each truth table in Appendix B.

As an aid to attaching physical significance to each truth table below, several conventions will be used. First, since the inputs to the RIS were logical variables which were derived from the system state variables, the truth condition of the logical variables is indicated for each section of the phase plane and the associated truth values of the functions A and F are indicated by a connecting arrow.

Second, "stick diagrams" of the dog are shown for each quadrant of the phase plane as a parallel descriptive notation. These diagrams show the approximate position of the dog's body relative to the table, the direction of the relative velocity, and the direction of the table motion (when needed) as explained in Figure 6.

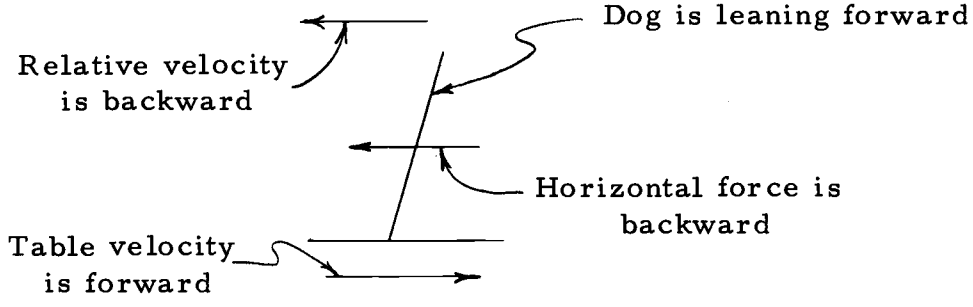

Figure 6. The "stick diagram" used to describe the state of the dog on the table. The forward direction is to the right wherever these diagrams are used.

A third convenience for the computer work was achieved by grouping the six variables into three ordered groups of two variables each and using a quarnary number code to represent the logical condition of the variable pairs. The groups used were WX VS EP. For example, the quarnary number 132 refers to the condition described by $\overline{W}X$ VS $E\overline{P}$, where a bar over the variable name indicates the logical inverse of the variable. The same coding was also used for the output variables A and F, in that order. In the simpler RIS logic systems where the leading variables were not used, the most significant digits of the number code were dropped from the notation since their truth values were irrelevent. In general, this notation will be combined with logical variable notation. However, where compactness is desired, the numerical coding will be used separately. (For clarification of the coding scheme, Tables 3 and 4 illustrate how the code was used.)

CNSS 0

The first RIS logic system, designated as the simple error system or RIS 0 (corresponding with CNSS 0), was a degenerate case since it used only one input variable P and one output variable F. (A was always "true".) The truth table appears as Table 1 and the phase plane is given in Figure 7.

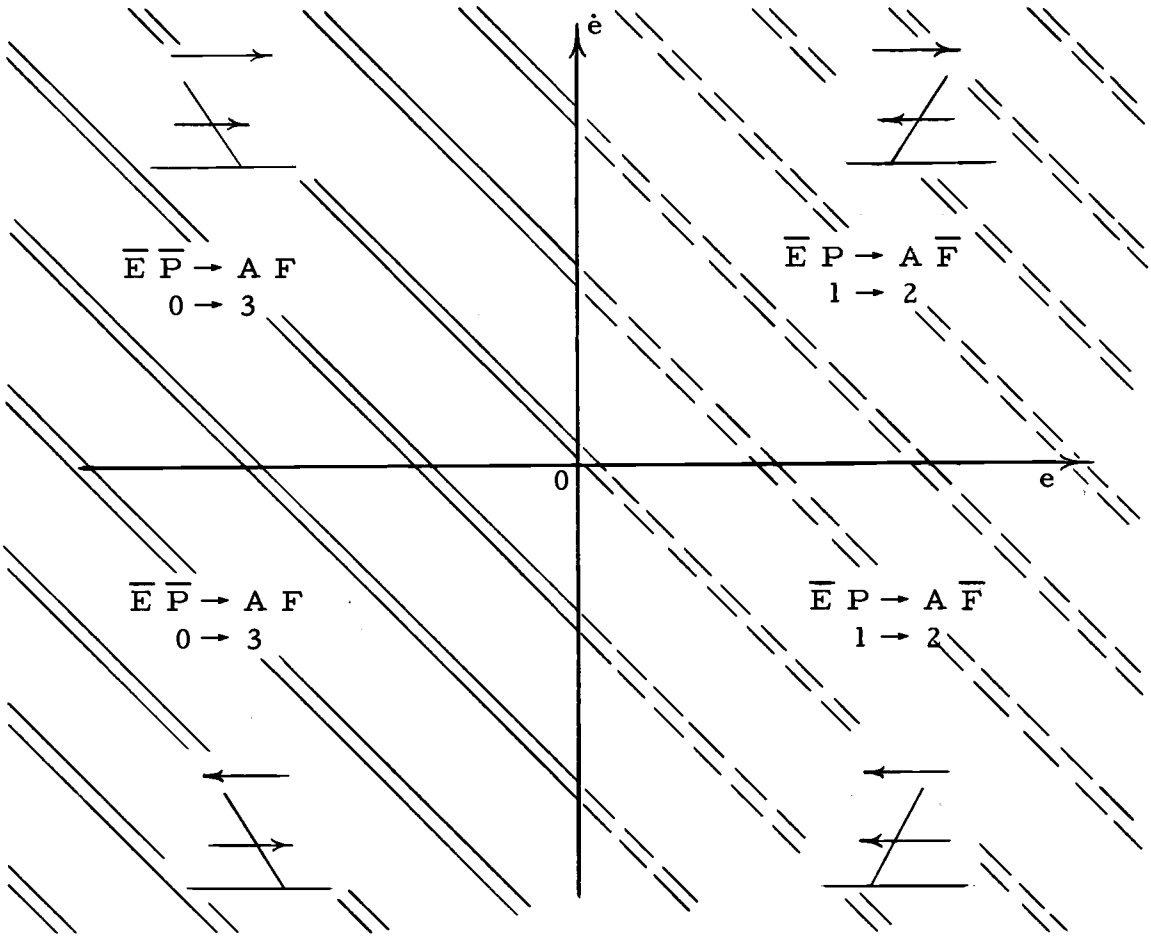

Figure 7. Phase plane logic pattern for the RIS 0 logic system. Solid crosshatching indicates the active-forward (AF) mode as opposed to broken crosshatching for the active-backward (A $\overline{F}$) mode. The symbol → has the following meaning: The given combination of truth values for the input variables results in the given combination of truth values for output variables.

Table 1. RIS 0 truth table.

Input condition		Output condition	
$\overline{P}$	0	A F	3
P	1	A $\overline{F}$	2
Logical functions:		A = u	
		F = $\overline{P}$	

CNSS 1

Considering a second RIS logic system, we desire that for the condition of a stationary table and a small error magnitude, only small muscle effort should be exerted to maintain proper posture control. This result was obtained by causing the output variable A to be "false" whenever the error magnitude was small, thus reducing the muscle tension. The RIS 1 logic system was used to form CNSS 1, which was basically equivalent with CNSS 0 except that the horizontal force capability was reduced for small errors. See Table 2 and Figure 8.

CNSS 2

The next RIS logic system, RIS 2, was known as the error-velocity system. The truth table, Table 3, shows that there were 16 (quarnary 100) possible input states, all of which could occur in the physical system. A study of the phase plane of Figure 9 is perhaps more informative. Whenever the system's state point was within the small region about the origin, the operation of the control logic (the RIS) was equivalent with the simple error system (RIS 0) except that the passive mode existed (A was always "false"). Outside this region, however, considerably different action occurred. The significance of each region will be discussed later.

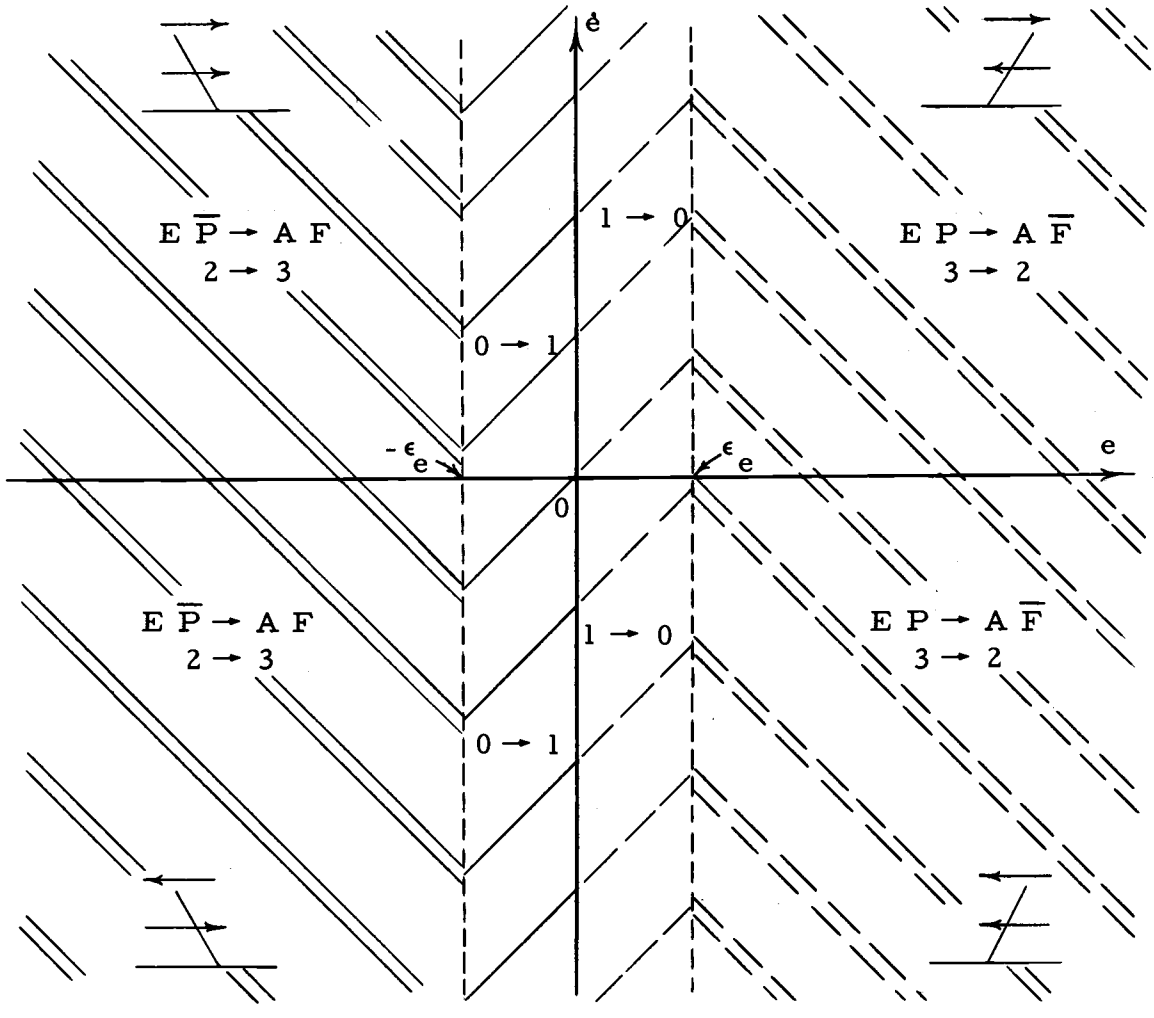

Figure 8. Phase plane logic pattern for the RIS 1 logic system. The crosshatch code is as follows: Single lines--passive mode ($\overline{A}$); double lines--active mode (A); solid lines--forward (F); broken lines--backward ($\overline{F}$).

Table 2. RIS 1 truth table.

Input condition		Output condition	
$\overline{E}\,\overline{P}$	0	$\overline{A}$ F	1
$\overline{E}$ P	1	$\overline{A}\,\overline{F}$	0
E $\overline{P}$	2	A F	3
E P	3	A $\overline{F}$	2

Logical functions: $A = E$
$F = \overline{P}$

Table 3. RIS 2 truth table.

Input condition		Output condition	
$\overline{V}\ \overline{S}\ \overline{E}\ \overline{P}$	00	$\overline{A}\ F$	1
$\overline{V}\ \overline{S}\ \overline{E}\ P$	01	$\overline{A}\ \overline{F}$	0
$\overline{V}\ \overline{S}\ E\ \overline{P}$	02	$A\ F$	3
$\overline{V}\ \overline{S}\ E\ P$	03	$A\ \overline{F}$	2
$\overline{V}\ S\ \overline{E}\ \overline{P}$	10	$\overline{A}\ F$	1
$\overline{V}\ S\ \overline{E}\ P$	11	$\overline{A}\ \overline{F}$	0
$\overline{V}\ S\ E\ \overline{P}$	12	$A\ F$	3
$\overline{V}\ S\ E\ P$	13	$A\ \overline{F}$	2
$V\ \overline{S}\ \overline{E}\ \overline{P}$	20	$A\ F$	3
$V\ \overline{S}\ \overline{E}\ P$	21	$A\ F$	3
$V\ \overline{S}\ E\ \overline{P}$	22	$A\ F$	3
$V\ \overline{S}\ E\ P$	23	$\overline{A}\ \overline{F}$	0
$V\ S\ \overline{E}\ \overline{P}$	30	$A\ \overline{F}$	2
$V\ S\ \overline{E}\ P$	31	$A\ \overline{F}$	2
$V\ S\ E\ \overline{P}$	32	$\overline{A}\ F$	1
$V\ S\ E\ P$	33	$A\ \overline{F}$	2

Logical functions:

$$\overline{A} = \overline{V}\ \overline{E} + V\ S\ E\ \overline{P} + V\ \overline{S}\ E\ P$$

$$\overline{F} = P\ E + P\ \overline{V} + V\ S\ \overline{E}$$

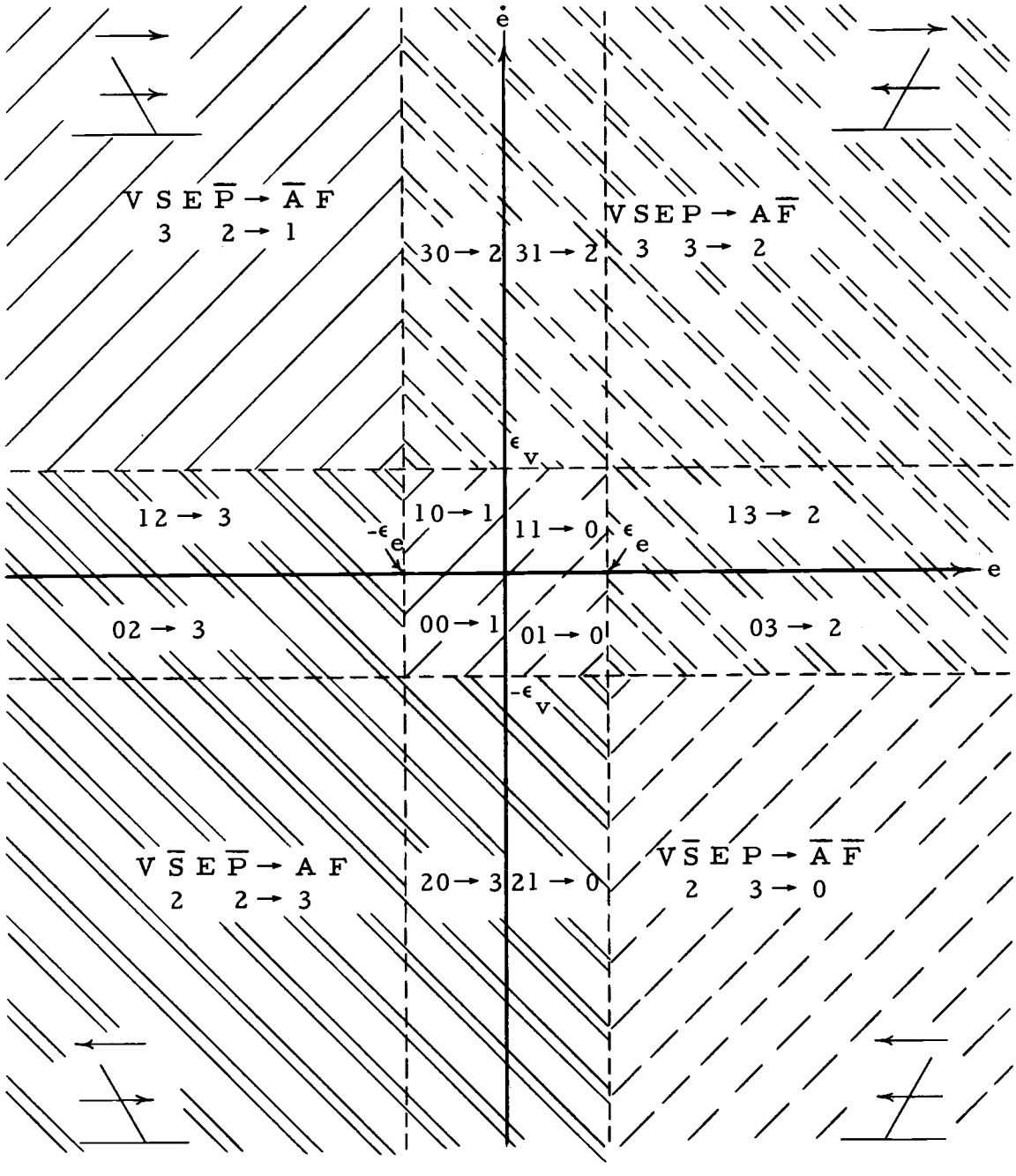

Figure 9. Phase plane logic pattern for the RIS 2 logic system. See the caption for Figure 8 for an explanation of the crosshatch code.

CNSS 3

The most elaborate logic system used all six available logical variables as inputs, these being derived from the analog variables $(y-x)$, $(\dot{y}-\dot{x})$, and $\dot{x}$. It is designated as RIS 3, corresponding with the truth table of Table 4 and the phase planes of Figure 10.

To visualize how this system related to the phase plane, we must note that the analog variable $\dot{x}$ does not appear as a phase plane coordinate. In effect, this adds a third dimension. To resolve this situation, two separate phase plane logic patterns are presented. One plane represents the logic for forward table motion (X "true", $\dot{x} > 0$) while the other is for backward table motion (X "false", $\dot{x} < 0$). The anterior end of the animal determines the forward direction.

Table 4. RIS 3 truth table.

Input condition		Output condition	
$\overline{W}\,\overline{X}\,\overline{V}\,\overline{S}\,\overline{E}\,\overline{P}$	000	$\overline{A}$ F	1
⋮	Same as RIS 2	⋮	
$\overline{W}$ X V S E P	133	A $\overline{F}$	2
W $\overline{X}$ $\overline{V}$ $\overline{S}$ $\overline{E}$ $\overline{P}$	200	...	
⋮	Not physically possible, $\overline{V} \rightarrow \overline{W}$		
W $\overline{X}$ $\overline{V}$ S E P	213	...	
W $\overline{X}$ V $\overline{S}$ $\overline{E}$ $\overline{P}$	220	A F	3
W $\overline{X}$ V $\overline{S}$ $\overline{E}$ P	221	A F	3
W $\overline{X}$ V $\overline{S}$ E $\overline{P}$	222	A F	3
W $\overline{X}$ V $\overline{S}$ E P	223	A $\overline{F}$	2
W $\overline{X}$ V S $\overline{E}$ $\overline{P}$	230	A $\overline{F}$	2
W $\overline{X}$ V S $\overline{E}$ P	231	A $\overline{F}$	2
W $\overline{X}$ V S E $\overline{P}$	232	A $\overline{F}$	2
W $\overline{X}$ V S E P	233	A $\overline{F}$	2
W X $\overline{V}$ $\overline{S}$ $\overline{E}$ $\overline{P}$	300	...	
⋮	Not physically possible, $\overline{V} \rightarrow \overline{W}$		
W X $\overline{V}$ S E P	313	...	
W X V $\overline{S}$ $\overline{E}$ $\overline{P}$	320	A F	3
W X V $\overline{S}$ $\overline{E}$ P	321	A F	3
W X V $\overline{S}$ E $\overline{P}$	322	A F	3
W X V $\overline{S}$ E P	323	A F	3
W X V S $\overline{E}$ $\overline{P}$	330	A $\overline{F}$	2
W X V S $\overline{E}$ P	331	A $\overline{F}$	2
W X V S E $\overline{P}$	332	A F	3
W X V S E P	333	A $\overline{F}$	2

Logical functions:

(See Appendix B, p. 105).

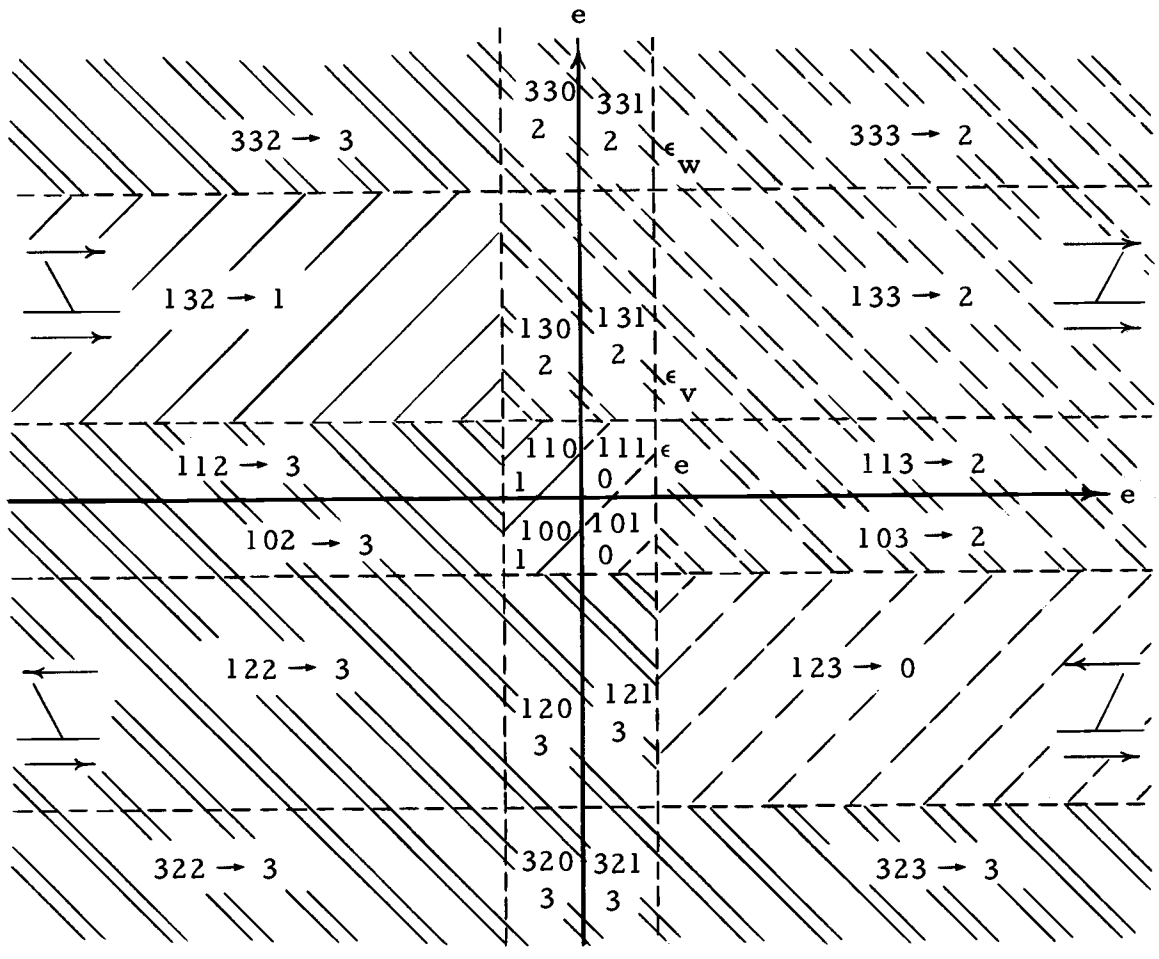

10A. Forward table motion.

Figure 10. Phase plane logic patterns for the RIS 3 logic system. Note that the direction of table motion cuases a change in the logic in certain regions. See Figure 8 for an explanation of the crosshatch code.

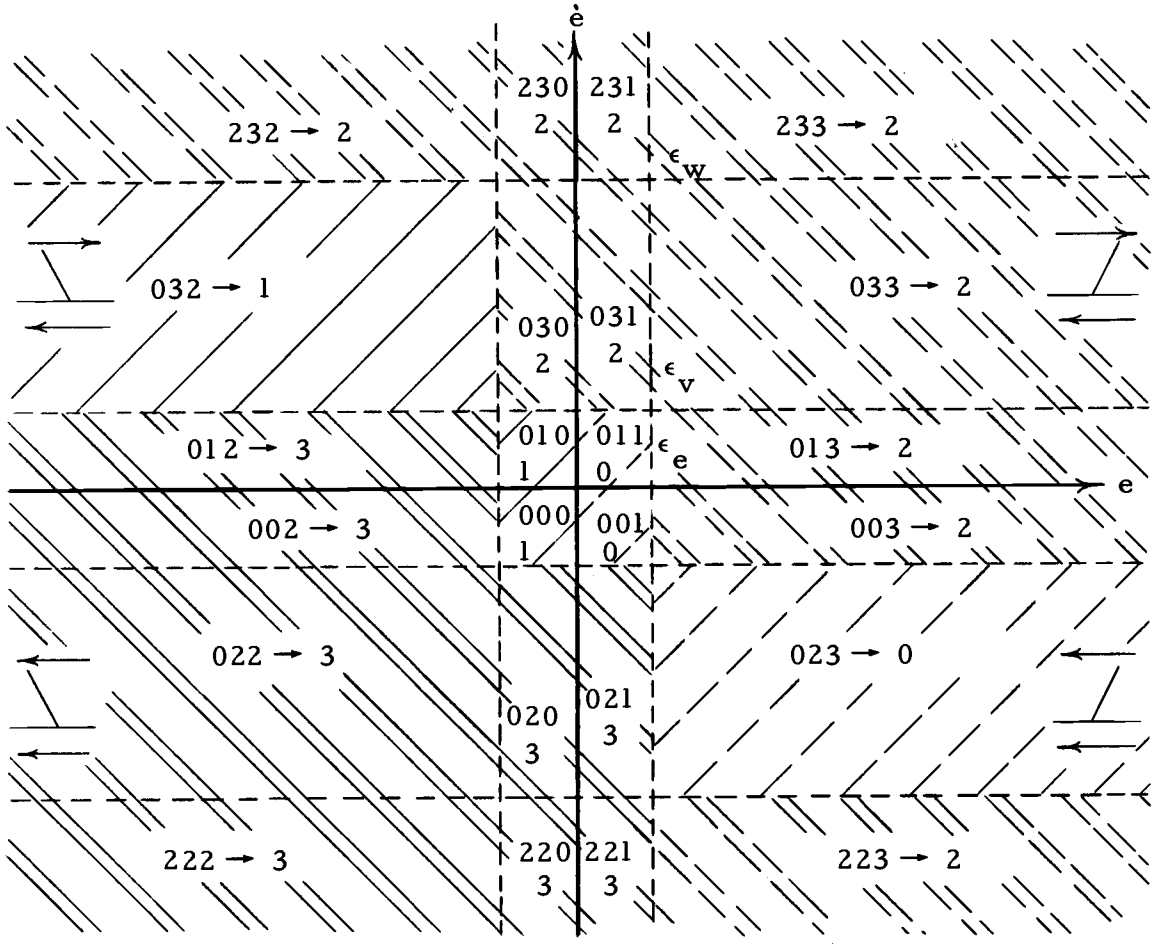

Figure 10B. Backward table motion.

III. DOG DATA

Before examining the various simulation systems resulting from combinations of the subsystems which have been presented, it seems appropriate to summarize the character of the data available for live dogs. The records are of a preliminary nature but serve to form a qualitative feeling for the action which occurred during experimental study.

A sample of the primary data which has been obtained from the dog is shown in Figure 11 [3]. Observe that at the frequency shown, the body moved considerably less than the table, meaning that the legs were allowed to swing quite freely under the body. Although the body movement was not sinusoidal, an intuitive feeling for the response of the body as a function of frequency can be gained from a plot of peak-to-peak amplitude versus frequency. (The meaning of these types of plots is discussed in Chapter V.) This plot is given as Figure 12 [3]. Subject to the same nonsinusoidal limitation, a plot of the equivalent phase lag for the fundamental is also given. These data were obtained from the records of only one dog but seemed to represent the basic characteristics which could be expected for different animals.

The slow drifting seen in Figure 11 appeared to a varying degree in several dogs and was of particular interest. The nonperiodic

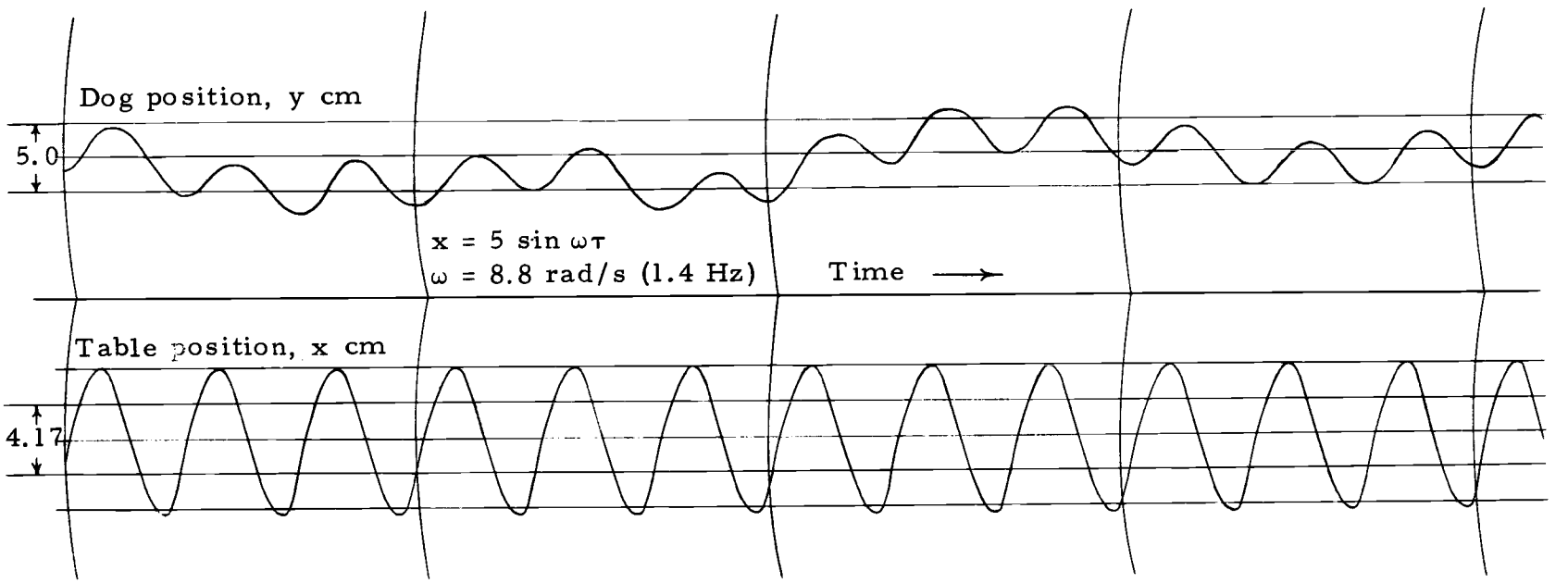

Figure 11. Movement of the dog relative to a fixed reference in response to sinusoidal table motion. This figure is an artist's copy of the original strip-chart recordings taken from Dog #9 of the UOMS experiment [3]. Notice that the body position displays a slow drift in addition to the attenuated fundamental response.

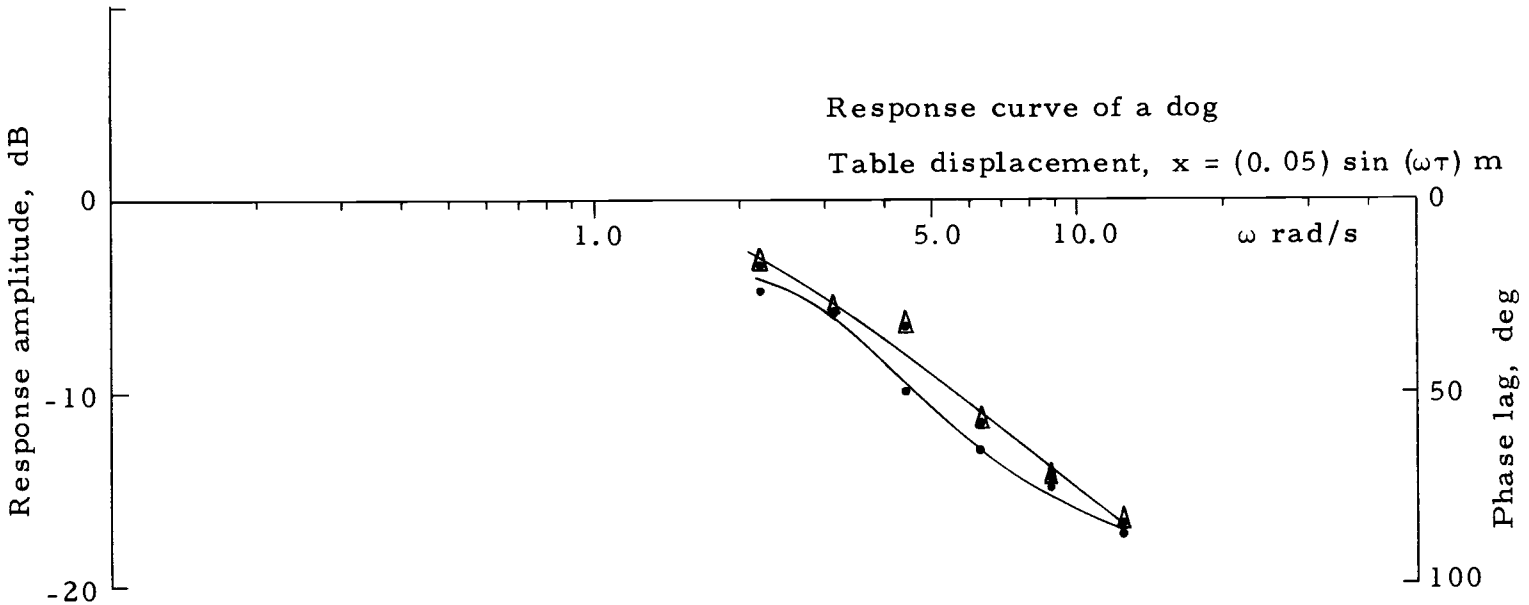

Figure 12. An amplitude-phase plot for a dog used in the UOMS experiment. The amplitude plot represents peak-to-peak displacement of the body as taken from data records similar to that shown in Figure 11. The phase plot represents the approximate phase lag of the fundamental component of the body movement, obtained from the same data records used for the amplitude plot [3].

drift became most evident above 1 Hz and seemed not to vary a great deal regardless of the table frequency. However, the nature of the drift varied more between different animals than did the other characteristics. In each case, the body appeared to drift unhindered until balance became critical at which time the drift changed direction. There is presently no acceptable explanation for this behavior, although the feeling remains that the animal was not able to maintain a constant volitional reference as the table movement became more pronounced.

Figure 13 shows a sample of another type of data record obtained from the dogs [3]. These are X-Y plots of table position versus dog position which are similar to the classical Lissajou plots. Since the dog did not move sinusoidally, the value of these plots is more qualitative than quantitative. This particular figure represents equivalent phase angles of about 35 and 50 deg lagging, taken at frequencies of 0.7 and 1.4 Hz, respectively.

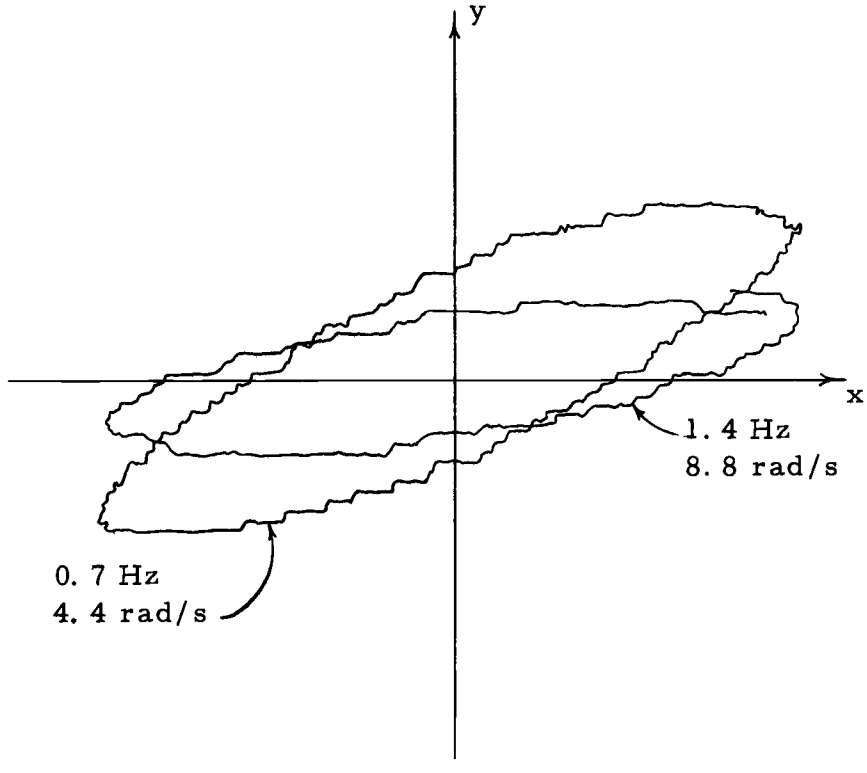

Figure 13. Dog position versus table position. This is an artist's copy of data recorded in the UOMS experiment [3]. Even though the body movement was not sinusoidal, these "Lissajou-like" figures were used to obtain a qualitative sense of phase lag and response amplitude.

IV. THE SIMULATION SYSTEMS

The final step in this simulation was to bring the three subsystems--the CNSS, the LMS, and the body simulator--together into a complete model. The following discussion presents each complete simulation model as it was originally developed. The characteristics and significance of each system are discussed in sequence below whereas the data records are included in the data catalog (Chapter V) which follows this section.

CNSS 0 Systems

The first and most simple system combined CNSS 0 with each of the LMS's. For the TLMS with $\alpha = 1$, this system was a simple linear case except for the presence of relative velocity feedback (viscous friction), as can be seen from Equation (6) below. Figure 15 of the data catalog, obtained from

$$\ddot{y} + k_d(\dot{y} - \dot{x})/m + k_t(y - x)/mh^2 = 0, \qquad (6)$$

shows an approximate gain-phase plot of the system for $k_d/m = 0.5/s$ and $k_t/mh^2 = 5.77/s^2$.

It is interesting to note that although the amplitude plot is only slightly different from that of a simple second order system ($\omega_n = 2.4 = \sqrt{5.77}$), the phase plot shows significant deviations above

$\omega = 3$ rad/s. By rewriting Equation (6) as Equation (7), we can see that because the result is,

$$\ddot{y} + k_d(\dot{y})/m + k_t(y)/mh^2 = k_d(\dot{x})/m + k_t(x)/mh^2 \ , \qquad (7)$$

the effect of the relative velocity feedback is equivalent to adding an input term proportional to $\dot{x}$ to a simple second order system. Equation (8) shows the resulting input terms when $x = a \sin \omega\tau$.

$$k_d(\dot{x})/m + k_t(x)/mh^2 = \frac{k_d}{m}[a\omega \cos \omega\tau] + \frac{k_t}{mh^2}[a \sin \omega\tau]$$

$$= a[\frac{k_d}{m}\omega \sin (\omega\tau + \pi/2) + \frac{k_t}{mh^2} \sin \omega\tau] \qquad (8)$$

Clearly, the presence of the $\sin (\omega\tau + \pi/2)$ term accounts for the increasing phase plot of the system. By substituting typical values for the constants and setting $\omega = 11.54$ rad/s, the following result is obtained

$$\frac{k_d}{m}(\dot{x}) + \frac{k_t}{mh^2}(x) = 5.77\ (a)[\sin (\omega\tau + \pi/2) + \sin \omega\tau]$$

$$= 5.77\ (a)[\sqrt{2} \sin (\omega\tau + \pi/4)], \qquad (9)$$

where the trigonometric identity,

$$\sin x + \sin y = 2 \sin \frac{1}{2}(x+y) \cdot \cos \frac{1}{2}(x-y) \ ,$$

has been employed with $x = (\omega\tau + \pi/2)$ and $y = \omega\tau$. Hence, at

ω = 11.54 rad/s, the expected phase lag will be 45 deg less than that of a simple linear second order system and the amplitude will be increased by 3 dB (20 log $\sqrt{2}$). The computer simulation gave observed values of 133 deg phase lag and an amplitude of -23.7 dB as compared with the theoretical values of 134 deg and -23.8 dB, respectively.

From this we may conclude that both viscous friction and relative velocity feedback via sensory channels may contribute to the increasing phase characteristic observed in the dog. Two other factors, the predictive capability of the CNS and regenerative feedback, may also account for a significant portion of the phase gain over a second order system. This point is emphasized since joint friction is expected to be quite small.

In considering the predictive function of the CNS in postural control, a complication appears in that relative velocity feedback produces effects which are similar to predictive control. Intuitively, this is true because the velocity at a given time is a good predictor of the change in position expected by some future time. A careful evaluation of the dog's behavior will be necessary to separate predictive control from joint friction and regenerative feedback since any one of them may produce increasing phase characteristics.

The different muscle characteristics represented by each LMS did not cause as much variation in the data as might have been

expected, except near the resonance. The CFLMS showed a lower peak in the response curve and slightly decreased phase lag. Because the CFLMS was a nonlinear element, the output response was not sinusoidal.

CNSS 1 Systems

Having briefly considered the basic system, we can follow the evolution of the different RIS's and their associated systems and note how each one altered the data obtained. The first objection to the above simulation was that the approximate resonance at 2.4 rad/s was much higher than what was observed in the dog during quiet standing, although it is reasonably close to the "corner point" shown by the dog during table movement. One reason for this might be that the muscle tension required during table excursions was certainly greater than that required during quiet standing. The method used to achieve reduced muscle tension was to set an error level ϵ_e near zero so that a logic variable E could be defined as "true" for error magnitudes above this level and "false" for magnitudes below this level. The first system including this feature, CNSS 1, was organized so that the muscle tension control variable A was "false" whenever the error was small, thus reducing the tension by a factor $1/\beta$. Hence, the natural resonance was reduced by a factor of $1/\sqrt{\beta}$.

Observations of this system using $\epsilon_e = 0.005$ m, showed that

the inclusion of a single error switching level did not really improve the quiet standing pattern significantly. After a minor disturbance, the system oscillated between the positive and negative error levels at a frequency greater than the natural resonance for reduced muscle tension. Although the concept of reduced muscle activity when small position errors existed was justified, this oversimplification was not particularly useful. The actual system in the PCS used for postural control during small displacements appears to be different from the system used during larger displacements. In general, we are concerned with larger disturbances, hence, we leave this point unresolved.

The sinusoidal responses of this system (CNSS 1) with each LMS were essentially the same as for the preceding cases, as would be expected. With the CFLMS, the limit cycle oscillations between the error levels were more pronounced and persisted during low frequency table movements.

CNSS 2 Systems

By analyzing what occurred during oscillation cycles of the CNSS 0 systems, we desire to find some control pattern which will remove the resonant peak from the gain plot of Figure 15. Figure 17 shows which regions of the phase plane contained the system state point over several cycles of table movement. Observe that at the

positive and negative limits of table travel the state point enters the second and fourth quadrants, respectively. According to the control logic of RIS 0, for a state point in quadrant II the LMS was in the active-forward mode. Since the table began moving backward in quadrant II, we see that the LMS was still producing a forward directed force when the table was already beginning quite rapid backward motion. Because the force was directed forward the relative velocity increased significantly, causing considerable overshoot as evidenced by the amplitude peak in the response gain curve.

The logic pattern for RIS 2 altered the above conditions so that in quadrant II, the LMS was in the passive-forward mode rather than the active-forward mode, whenever the relative velocity magnitude was greater than a small value ϵ_v and the error magnitude was greater than ϵ_e. (Similarly, quadrant IV produced the passive-backward mode.) This decreased the muscle tension, and hence, the horizontal force during the time that a high relative velocity had been developed previously and had resulted in the overshoot and amplitude peak.

The RIS 2 pattern constituted a mild form of prediction based on the relative velocity as previously discussed. The general suppression of the resonant amplitude peak and the decreased response above 1.5 rad/s were accompanied by a small decrease in the phase lag. (See Figure 19.) As expected, the amount of relative velocity

feedback (damping or friction) did not affect the response amplitude in the region of the resonance nearly as much as previously. Variations in the phase lag for different amounts of relative velocity feedback were about the same as observed with CNSS 0 systems.

The changes between CNSS 0 and CNSS 2 systems appeared much the same as if the damping had been increased considerably. Effectively, reducing the acceleration in quadrants II and IV was much the same as increasing the damping relative to $\dot{y}$. Changes in damping will effect the shape of the response amplitude curve near the resonance considerably more than is true for the phase lag curve. Since the effective damping was increased, changes in the relative velocity feedback (joint and muscle friction) were not as significant as when no other source of damping was present.

When examined with CNSS 2, the different LMS's displayed characteristics, relative to each other, which were very similar to those for CNSS 0 systems except for the changes noted above. The CFLMS persisted in its tendency to produce subharmonics of considerable magnitude. For frequencies near 4.3 rad/s, a subharmonic of one-half the fundamental was observed whenever the relative velocity feedback was small (k_d = 1 N · s/m).

CNSS 3 Systems

Having reduced the resonant peak in the response curve using

CNSS 2, the next modification of the control pattern was aimed toward reducing the phase lag. Although increasing the relative velocity feedback would have produced less phase lag, it has already been suggested that this effect (friction) was not expected to be very significant in the dog.

Figure 14 shows the location of the system state point in the phase plane relative to the table motion. In logic regions 32 and 23 (quadrants II and IV, respectively), the LMS was in the passive-forward or passive-backward mode, respectively, regardless of how large the relative velocity was or what direction the table was moving. With this control logic, it was possible for the table to begin reverse motion while the relative velocity was still a large positive value without taking any action to reduce the velocity.

The logic system of RIS 3 used two new logic variables, W and X. W was "true" for relative velocity magnitudes greater than ϵ_w and X was "true" whenever the table was moving forward ($\dot{x} > 0$). Using these new variables with $\epsilon_w = 0.05$ m/s, the control logic pattern was set so that in sections 32 or 23, for large relative velocities the LMS was in the active mode and the force was applied in the same direction as the table motion. This logic represents a stronger form of prediction based both on the table velocity and the relative velocity.

The results of these changes in the logic control are evident

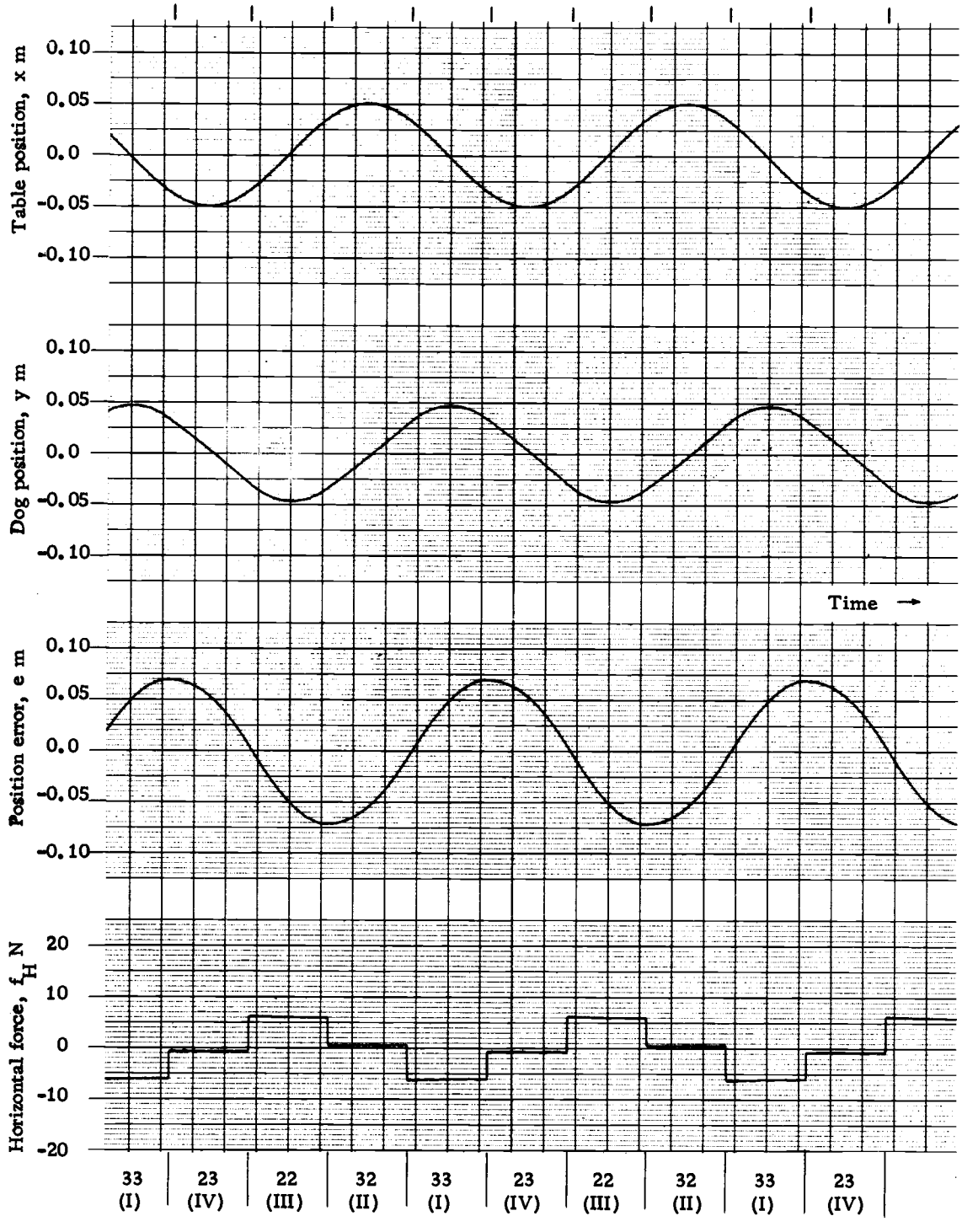

Figure 14. Typical response data for the CNSS 2;CFLMS system with $k_d = 1$ N·s/m and $\omega = 2.5$ rad/s. The logical switching points are evident by observing the horizontal force. These have been identified and may be correlated with the phase plane in Figure 9. Note that the narrow transition regions (20, 21, etc.) have been neglected.

from the gain-phase plots of Figure 22. The reduction of the phase lag may be understood by noting in Figure 25 that the force from the LMS is positive for forward table motion and negative for backward table motion. This is effectively a phase gain (prediction) of about 90 deg which agrees with the observed lags of about 90 deg rather than 180 deg for the higher frequencies. (See Figure 22.)

The CNSS 3; CFLMS simulation system gave data which more closely resembled that from the dog. At low frequencies the dog showed lower amplitudes and larger phase lags. For higher frequencies the phase lags were closer but the amplitudes for the dog were greater than for the simulation model and the asymptote was about 40 dB per decade rather than the desired 20 dB per decade observed in the dog. One new and interesting occurrence was the non-periodic "drift" which can be seen in Figure 23. Although the appearance of this drift should not be taken too seriously, it is perhaps significant that it is possible in a time-invariant system.

Comparison of the data for both the TLMS and the CFLMS using CNSS 3 shows that the best agreement with the desired results was obtained from the CFLMS. For the particular LMS parameters selected, the SLMS and TLMS produced essentially the same results. The VPLMS is considered separately below.

Recalling that the asymptote of the amplitude curve for the dog data in Figure 12 was about 20 dB per decade rather than the 40 dB

per decade of a simple second-order system, the possibility of introducing velocity-proportional feedback through the LMS was logically suggested. The logic control of the CNSS 3 systems was very nearly in phase with the relative velocity so that the switching between forward and reverse forces was properly timed to coincide with the change in direction of the relative velocity. Hence, the CNSS 3; VPLMS system was nearly equivalent with a system using only velocity-proportional feedback with no logic control.

The characteristics of this system were even more similar to the dog, as seen from Figure 26. Although the average error was not constant, the system did not drift in the manner of the CNSS 3; CFLMS system. Because the horizontal force from the LMS was a function of the relative velocity, the amount of feedback due to friction was much less significant than for any of the preceeding systems.

V. THE DATA CATALOG

Introduction

The data in this catalog have been selected to show the significant characteristics of each of the systems presented. The general aim has been to provide a qualitative description of the systems in addition to pointing out the differences between each. Since most of the systems discussed here were nonlinear, it must be remembered that the amplitude plots represent peak-to-peak amplitudes and the phase plots are approximations based on the dominance of the fundamental frequency component. A discussion of how to interpret the gain-phase plots follows below.

Since the descriptive plots for each of the systems show gain and phase versus frequency, it is natural to accept these as frequency-domain descriptions of the system. Unfortunately, this is not suitable. First, as mentioned above, the system responses are nonsinusoidal. An even more significant point follows, however.

Frequency-domain analysis of linear, minimum-phase systems is based on a uniqueness property which guarantees that any such linear system is uniquely and completely described by its frequency-domain representation. When the frequency-domain plots show nonminimum phase or when the system is known to be nonlinear, the uniqueness property fails. This means that the gain-phase versus

frequency plots given do not uniquely determine a particular time-domain system performance.

The conclusion of this discussion is simply that the plots given in this catalog should not be considered as frequency-domain descriptions of the systems. They are only given as point-by-point graphs of gain-phase versus frequency. These restrictions do not, however, exclude general descriptions of the curves in terms of the frequency-domain plots of more familiar minimum-phase systems.

In all of the following work, certain standard parameter and constant values were used. The body mass m was 20 kg throughout. The friction constant k_d was generally selected to be either $1\,N \cdot s/m$ or $10\,N \cdot s/m$, giving rise to a damping constant of either 0.0104 or 0.104, respectively, where applicable. The switching levels--ϵ_e, ϵ_v, and ϵ_w --were set at values of 0.005 m, 0.005 m/s, and 0.05 m/s, respectively. Those parameters which are related to the physical dimensions of the model for the LMS are specified in Figure A-1 of Appendix A. The constants for the TLMS, SLMS, and CFLMS were selected so that for an angular leg displacement of 5 deg, the horizontal force generated was 6 N. The VPLMS produced 6 N at 5 deg when the relative velocity was 0.097 m/s.

Presentation of Data

Gain and phase data for the first systems, CNSS 0; TLMS and

CNSS 0; CFLMS, are compared with a simple linear system in Figure 15. One characteristic not shown in the figure is that for the CFLMS system, at frequencies just below the amplitude peak, there was a range in which two responses were possible under identical conditions. It appeared that in one case the system would "lock" to the input signal, showing almost no error. If the system were then disturbed, a large error and phase lag would develope and be maintained, suggesting that the nonlinear nature of the CFLMS permitted two stable modes of operation for these specific frequencies. A sample of the strip chart recordings of this phenomenum is given in Figure 16. The small perturbations seen were evident whenever the CFLMS was used since the force generated by this simulator was never zero. Such a system will readily exhibit a limit cycle since there must be continual switching between positive and negative accelerating forces.

Short term ramp (step approximations) responses for these systems were of the same general nature as for a simple linear system and were definitely not like those shown by the dog. Note that when the table was stationary after the ramp was complete, $\dot{x}$ was zero, and in the case of the TLMS, the system equation was the same as for a simple second-order system.

Variations of α, the forward-reverse force ratio, did not produce major changes in the data. The general tendency was for the

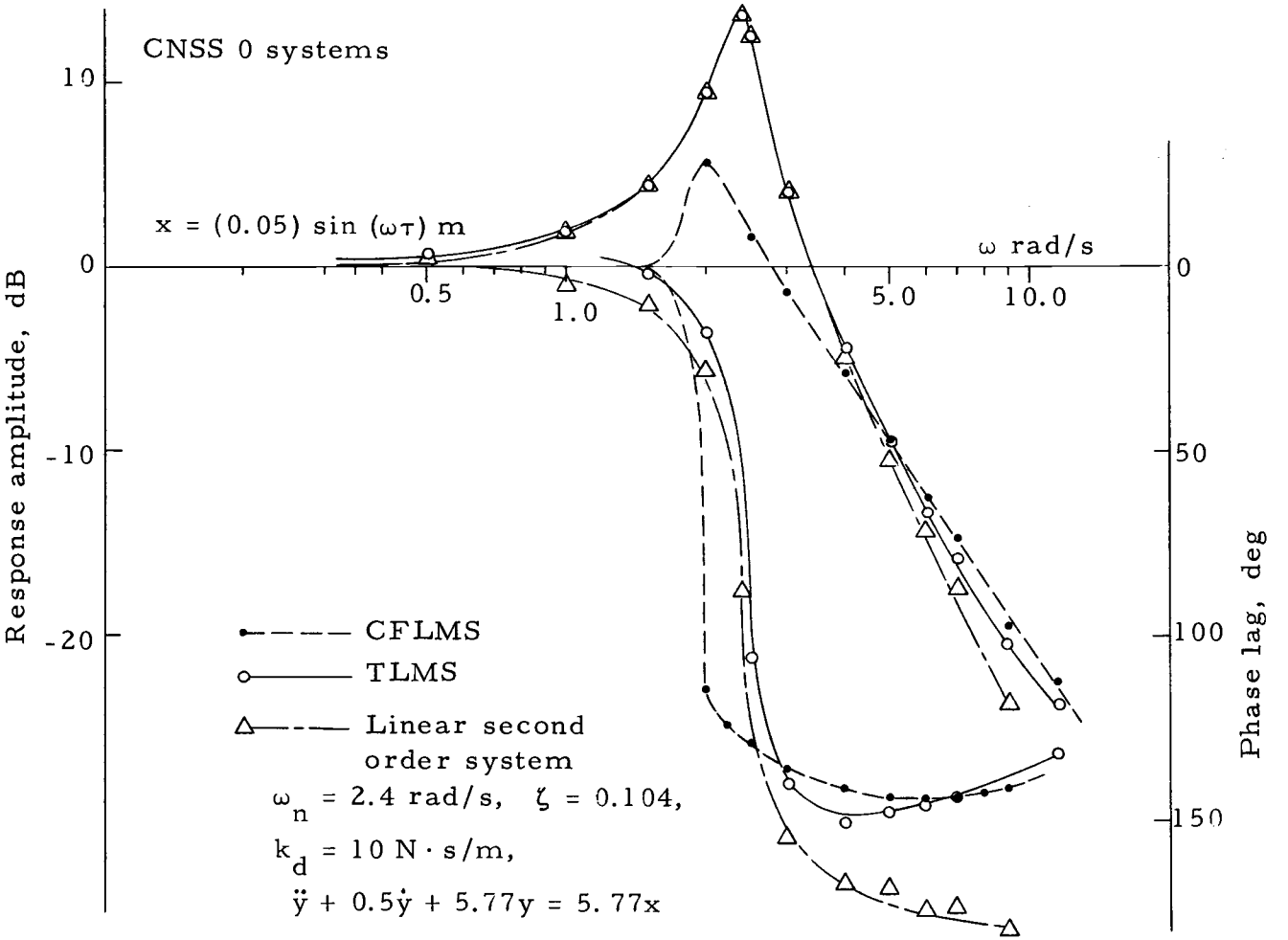

Figure 15. Amplitude and phase plots for CNSS 0 systems. Note that the amplitude curve of the CNSS 0; TLMS system is nearly the same as the linear system. The phase curves for both the TLMS and the CFLMS, however, become considerably different as the frequency increases.

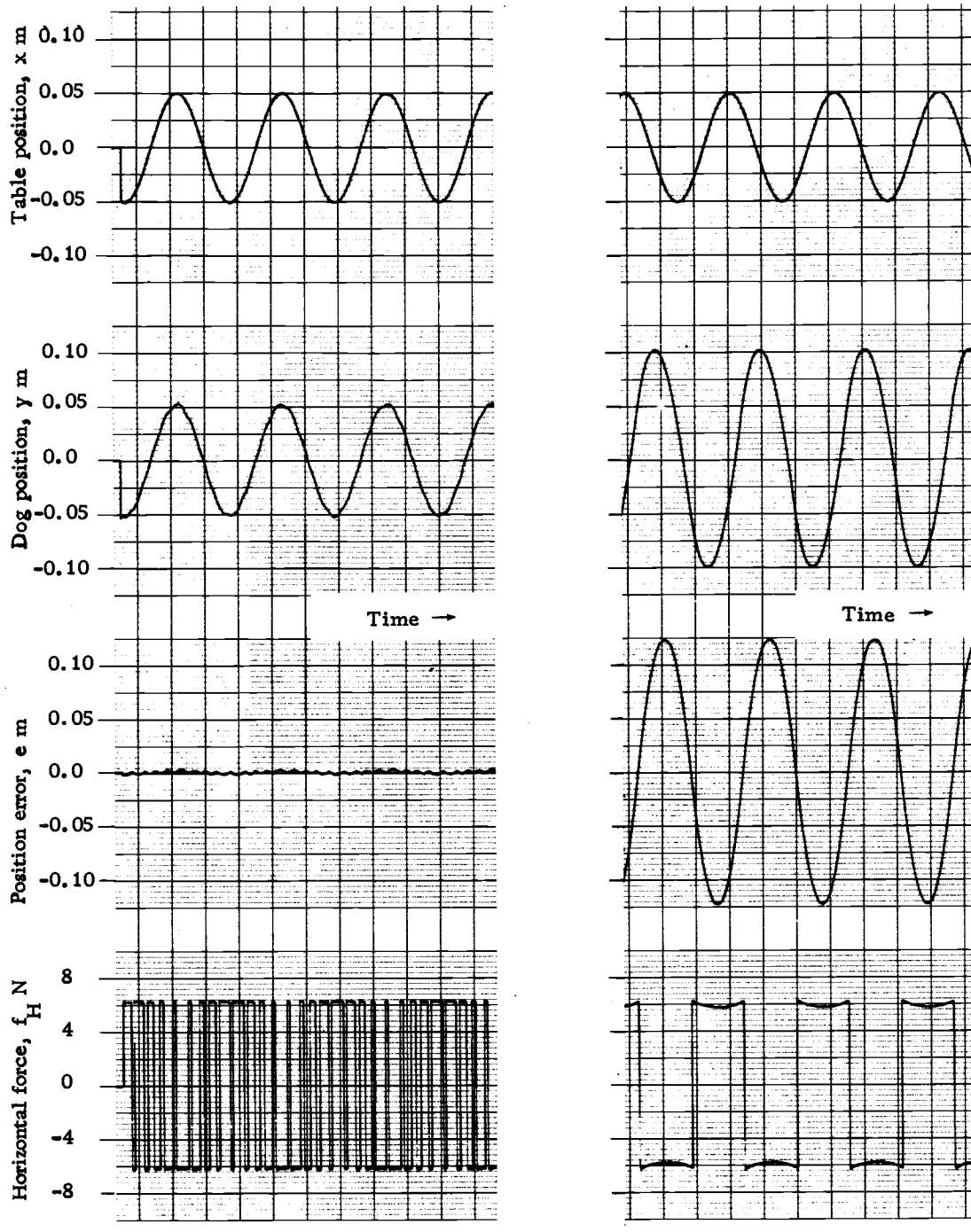

Figure 16. Double mode for the CNSS 0;CFLMS system. Although the system and parameters as well as the table behavior were exactly the same, these two distinct modes were observed for $\omega = 2$ rad/s. This type of nonunique phenomenon is one reason why nonlinear systems are difficult to analyze. All system parameters were the same as stated on page 61 except that the friction coefficient was slightly increased to $k_d = 12$ N·s/m.

body to lean in the direction in which the stronger force acted, i.e., for $\alpha = 2$, at a frequency of 4 rad/s, the average position was about 0.032 m forward. (See Figure 17.) As would be expected, the reduced acceleration for positive errors produced a nonsymmetric response cycle in which the positive portion showed a less pronounced curvature.

Although the tendency in the model for the average position of the center of mass to move forward for increasing values of α was intuitively expected, it is less clear what effect this nonsymmetry in the dog might produce. The fact that the dog likely uses a variable reference which may be both adaptive and stochastic was evidenced by the drift characteristic, which obscured activity that might otherwise have been apparent.

Figure 18 is a typical plot of y versus x for system CNSS 0; CFLMS at a frequency of 6 rad/s. It has been included so that later systems, also shown in the figure, may be compared with it.

No data from CNSS 1 systems are shown since there was very little difference between CNSS 1 and CNSS 0 systems. The limit cycle oscillations with the CNSS 1; CFLMS system during rest and low frequency table movements were of a lower frequency because of the reduced tension for small errors.

The gain-phase plots shown in Figure 19 are for CNSS 2 systems. Although the amplitude peaks have been suppressed and the

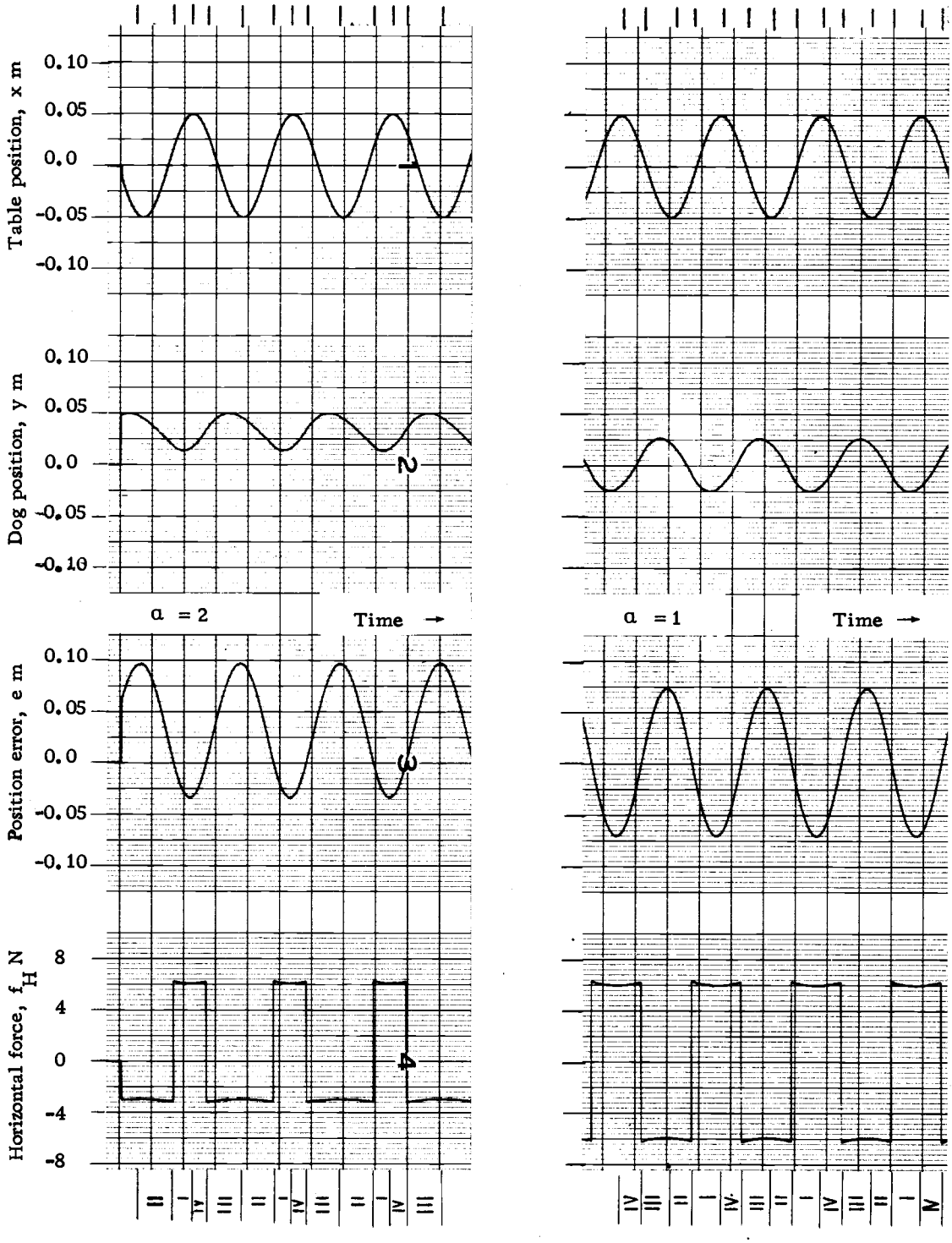

Figure 17. Comparison of the CNSS 0; CFLMS system response for two values of α, the forward-reverse force ratio, at $\omega = 4$ rad/s and $k_d = 10$ N·s/m. The nonsymmetry introduced in the response is intuitively what would be expected and can be explained by observing the nonsymmetry of the horizontal force. The quadrant numbers correspond with the phase plane quadrants in Figure 7.

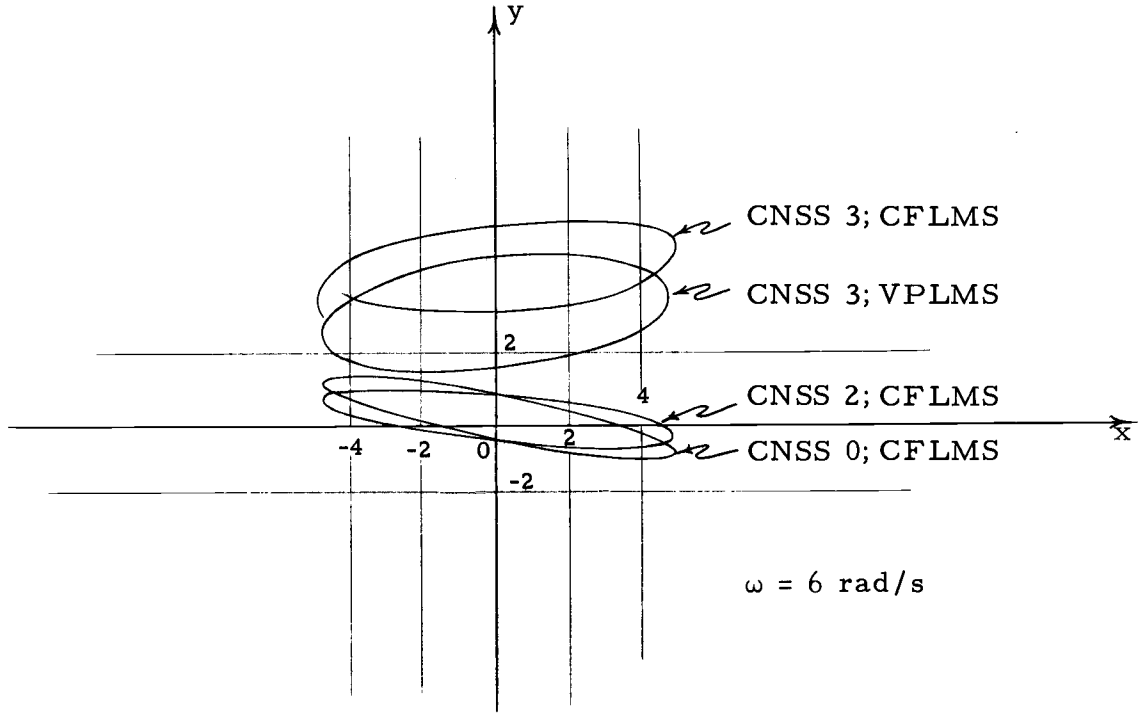

Figure 18. Comparison of the "Lissajou-like" plots of dog position versus table position for several systems. These figures are artist's copy of oscilloscope photographs and may be compared with Figure 13, which shows the equivalent data for the dog. Note that for the CNSS 3; CFLMS system the trace does not close as a result of the drift in the body response.

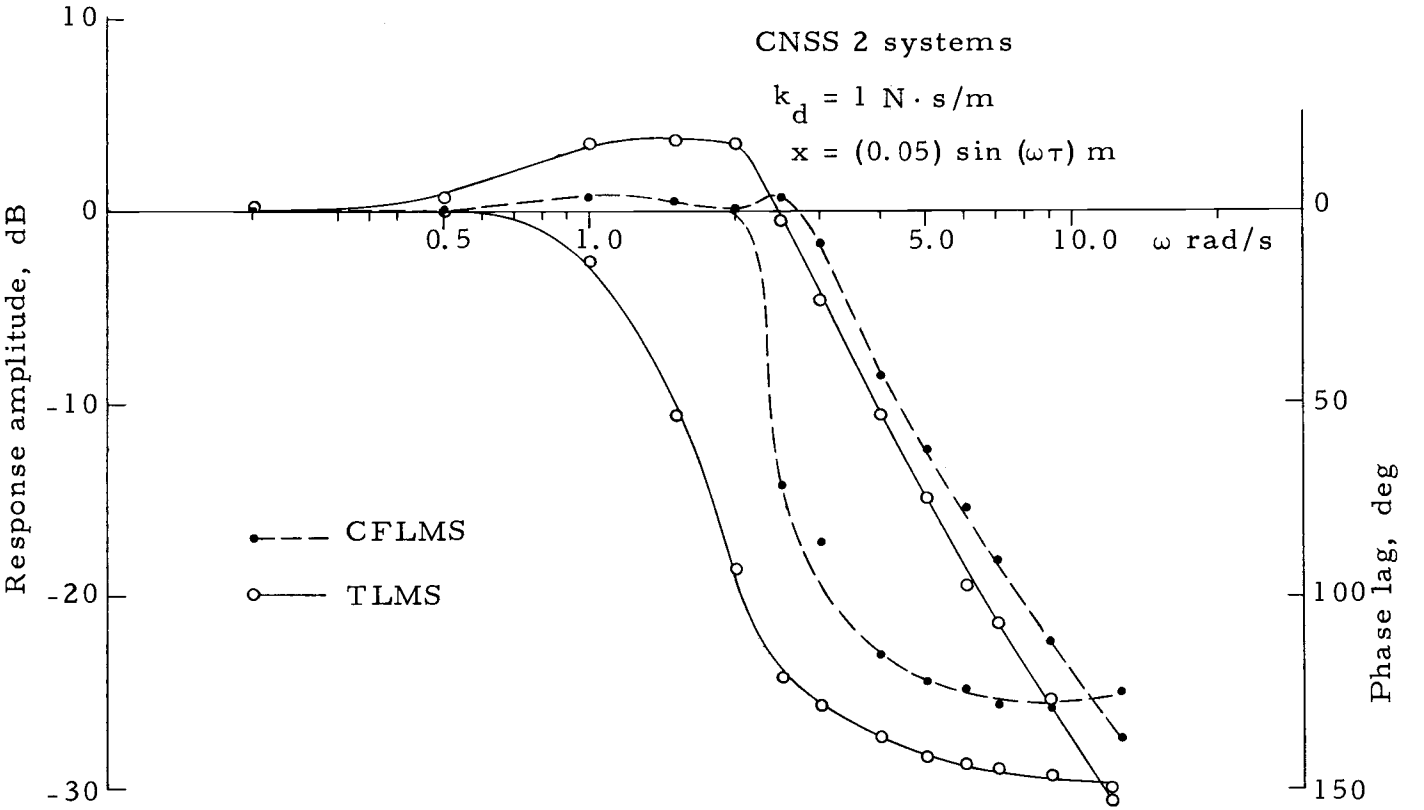

Figure 19. Amplitude and phase plots for CNSS 2 systems. Although the performance above 3 rad/s has not been changed much, the amplitude of the response near the natural resonance is significantly reduced. To a lesser degree, the phase lag has also been changed near resonance with the CNSS 2; CFLMS system.

phase lag reduced somewhat without the use of significant relative velocity feedback, the plots still show the major characteristics of a second-order system. The most meaningful result from the CNSS 2 systems was the reduction of the response amplitude near the resonance. A secondary result was that the system was not particularly sensitive to the amount of relative velocity feedback used.

Observing the reduction of the amplitude peak, an intuitive explanation is possible. By reducing the accelerating forces in quadrants II and IV, the damping was effectively increased greatly without reducing the force capability in quadrants I and III. Hence, the resonant peak was considerably decreased. The friction became less significant because the logic control already provided most of the damping. The phase lag characteristics, being less dependent on damping than the amplitude, were not as greatly changed and still reached much larger values than desired.

For sinusoidal responses, variation of a showed about the same results as for CNSS 0 systems, while changes in switching levels had little effect. The fast ramp responses were considerably improved since the overshoot was well damped by the control logic. Figure 20 shows a typical fast ramp response using $\epsilon_e = 0.005$ m and $\epsilon_v = 0.005$ m/s. The ramp responses were somewhat more sensitive to variation of the switching levels than the sinusoidal responses, although the changes were not extreme for level adjustments

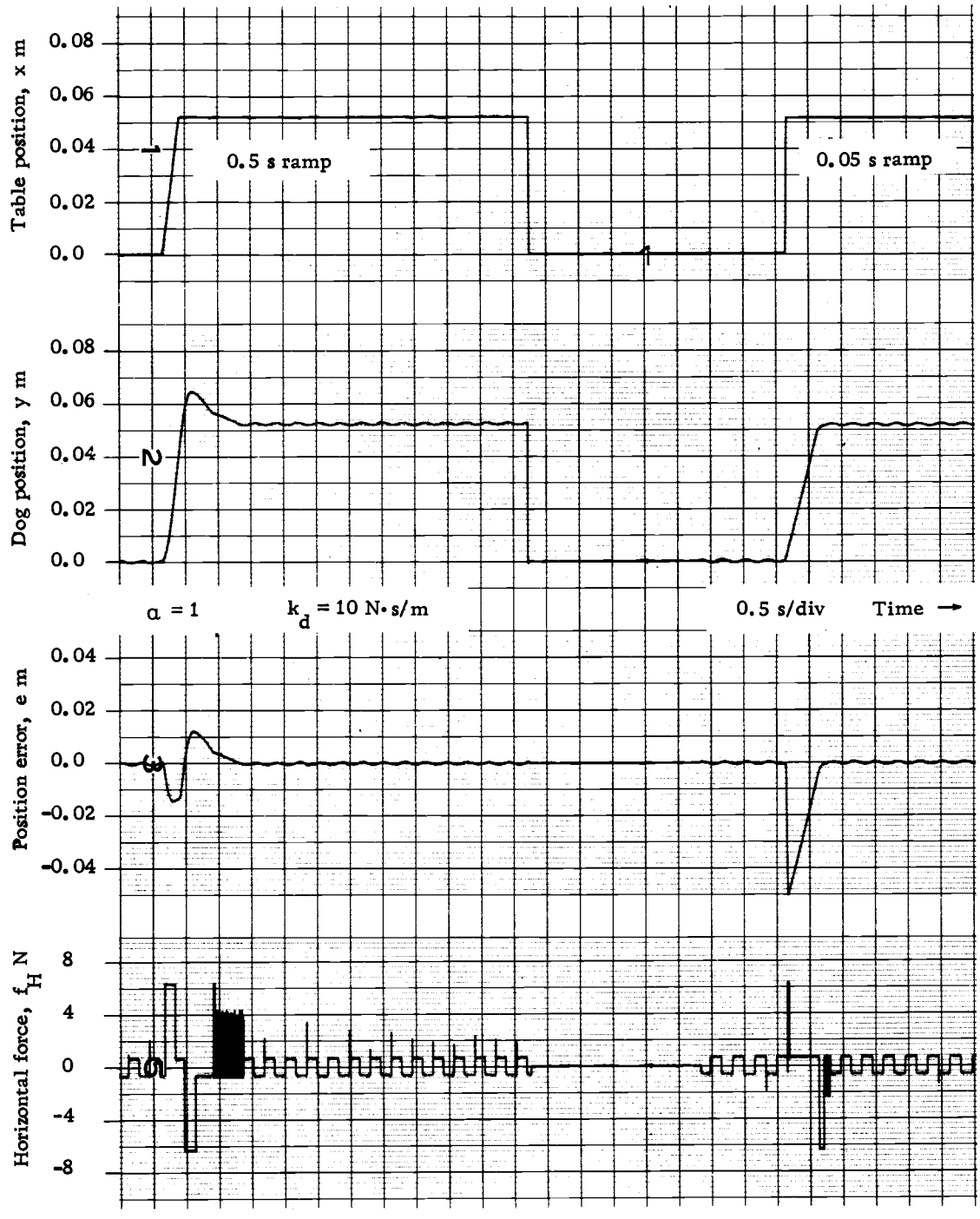

Figure 20. System responses for two different ramp displacements. The first response is for a 0.5 s, 0.05 m ramp and the second for a 0.05 s, 0.05 m ramp. The definite change in these responses reflects the nonlinear nature of the system. It appears that the shorter ramp is a suitable approximation to a step function for this system.

of nearly 100 percent. Even greater variation of the levels greater than 100 percent had little effect on the sinusoidal responses.

A system characteristic resulting from use of discrete logic switching levels is shown in Figure 21. During relatively slow table movements, the state point for CNSS 2 and CNSS 3 systems tended to follow the switching levels ϵ_e and ϵ_v around the origin of the phase plane. Since the analog-to-digital comparators had very sharply defined switching levels, a rapid limit cycle appearing much like noise developed. The evidence of this may be seen in the force pattern of Figure 21 where the rapid chatter between the active and passive force modes is evident. This phenomenum occurred most readily when the relative velocity was near ϵ_v. The frequency of the chatter was a function of the switching speeds of the analog-to-digital comparators and the electronic switches. The tendency to chatter was much more pronounced with the CFLMS since the most abrupt changes in force upon switching occurred when using this LMS.

The gain and phase data for CNSS 3 systems are presented in Figure 22. Despite the reappearance of a significant resonant amplitude peak for the TLMS, the reduced phase lag is sufficient to suggest an overall improvement in the data. For the TLMS, the amplitude near resonance was very sensitive to the amount of relative velocity feedback, a characteristic that was not true of the CFLMS. In both cases, however, the phase lag above resonance was almost unaffected

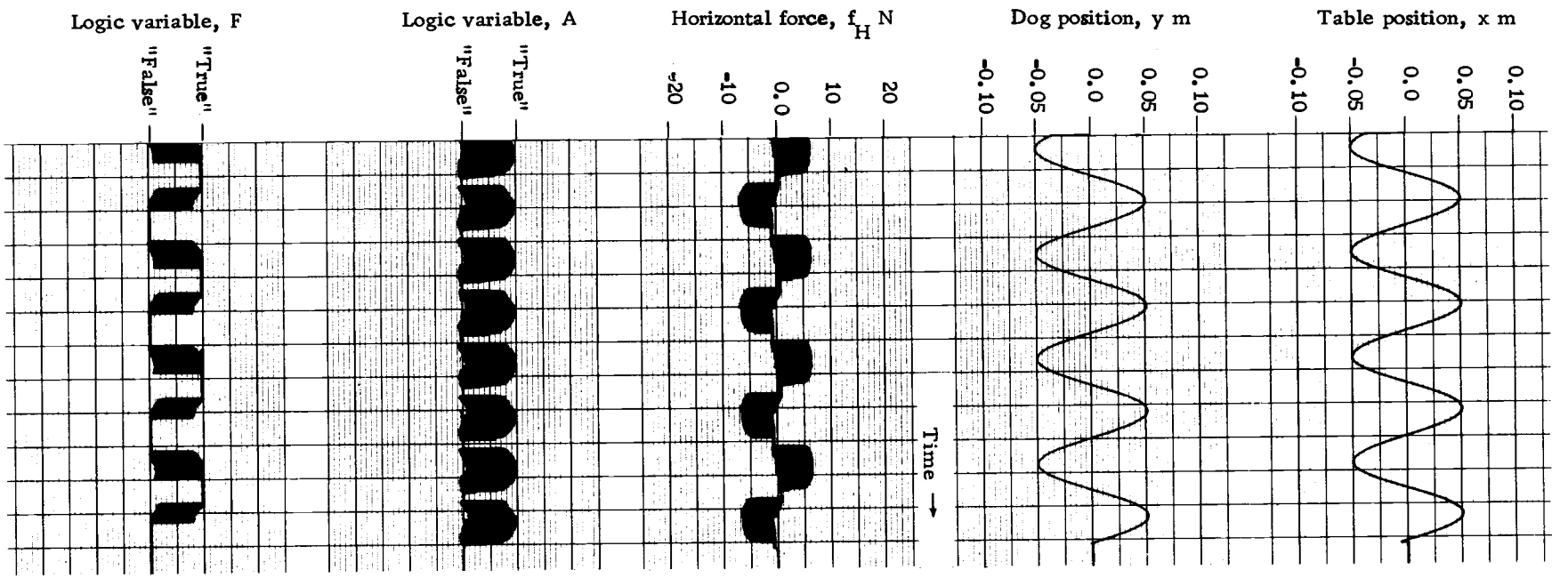

Figure 21. Logic chatter using the CNSS 2; CFLMS system. This chatter is a rapid limit cycle of the analog-to-digital comparators and logic elements. Although the only frequency shown is 2 rad/s, this phenomenon was observed with several of the systems and over a range of frequencies near 2 rad/s.

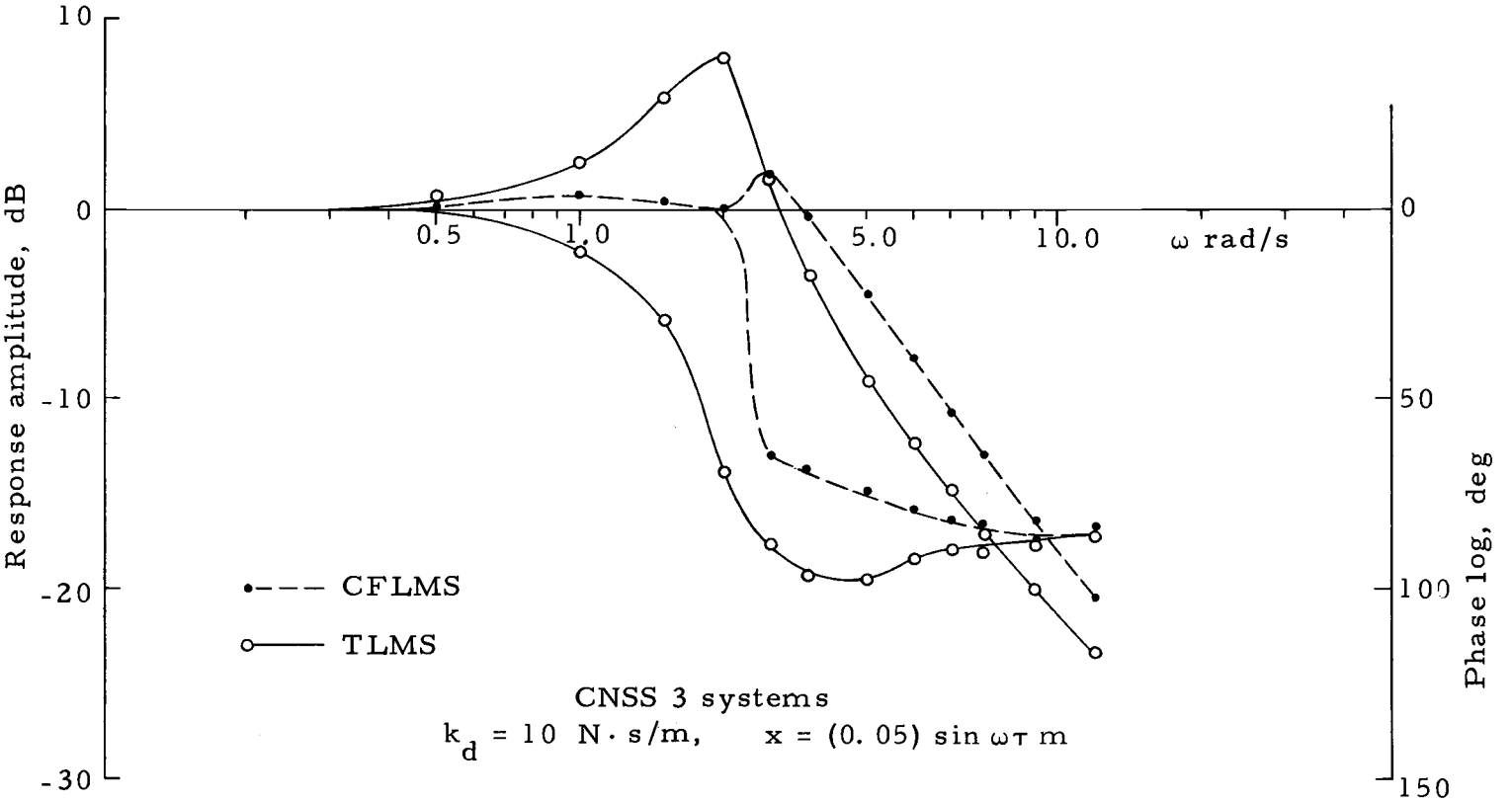

Figure 22. Amplitude and phase plots for two CNSS 3 systems. Using the TLMS, a definite amplitude peak can be seen while the CFLMS gives a quite different result more like the CNSS 2 systems. The significant change is that the phase lag does not exceed 100 deg at any time. These systems were not very sensitive to friction or switching level changes.

by changes in the realtive velocity feedback.

The CNSS 3 systems, in addition to showing strongly increasing phase data, possessed a totally unexpected "drift" characteristic which is seen in Figure 23. Although the drifting was most pronounced when there was little or no relative velocity feedback (no friction), the tendency persisted even for $k_d = 10$ N · s/m. The CFLMS was much more prone to this condition than was the TLMS. Values of α other than 1 greatly accentuated the drift tendency.

To see how the drift was developed, we refer to Figure 24 which shows the condition of the logic control variables A and F superimposed on an error cycle in the phase plane. It is clear that the curve can be moved horizontally to either side of center without changing the timing of the control logic switching as long as the path of the state point stays outside of the region where $|e| < \epsilon_e$ and $|\dot{e}| < \epsilon_w$. Intuitively, what this means is that within a pair of limits, the control logic timing is determined by the relative velocity rather than by the error (relative position), i. e., the control logic is velocity sensitive more than position sensitive.

Looking further, we see that the symmetric pattern of forward and reverse forces was possible regardless of moderate average errors because the force in logic regions 232 and 323 (quadrants II and IV of Figure 10B and 10A, respectively) was applied in the direction of the error, rather than opposite the error. Figure 24

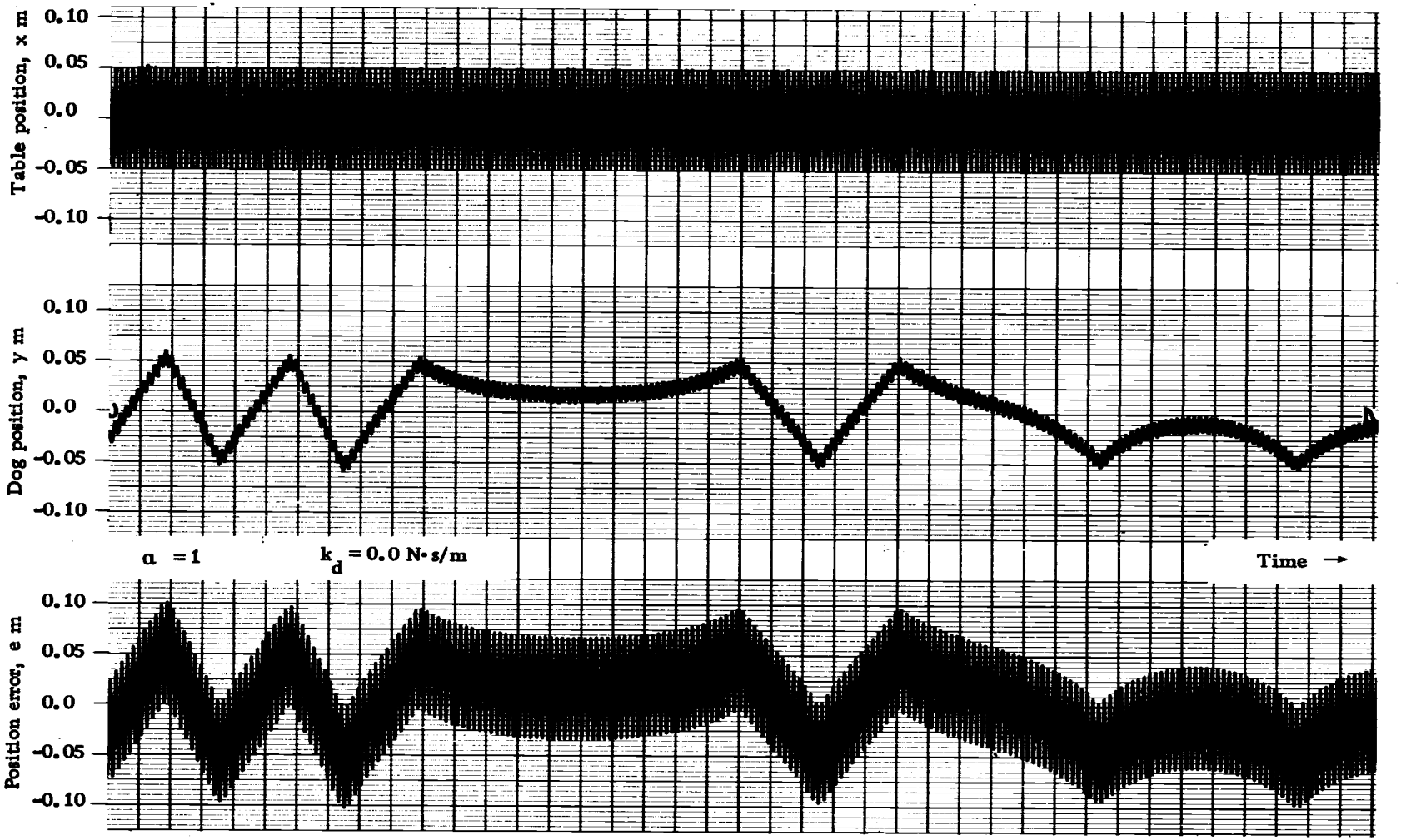

Figure 23. An example of the "drift" with the CNSS 3;CFLMS system. The data shown here were recorded with an input frequency of 7 rad/s using no friction. Since the rate of drift seemed to remain constant with table frequency, the appearance is quite different at lower frequencies. The triangle wave at the left seemed to be repeated quite often with more curious sections coming inbetween these sections. Although these data were recorded for long periods, a basic periodicity was never found.

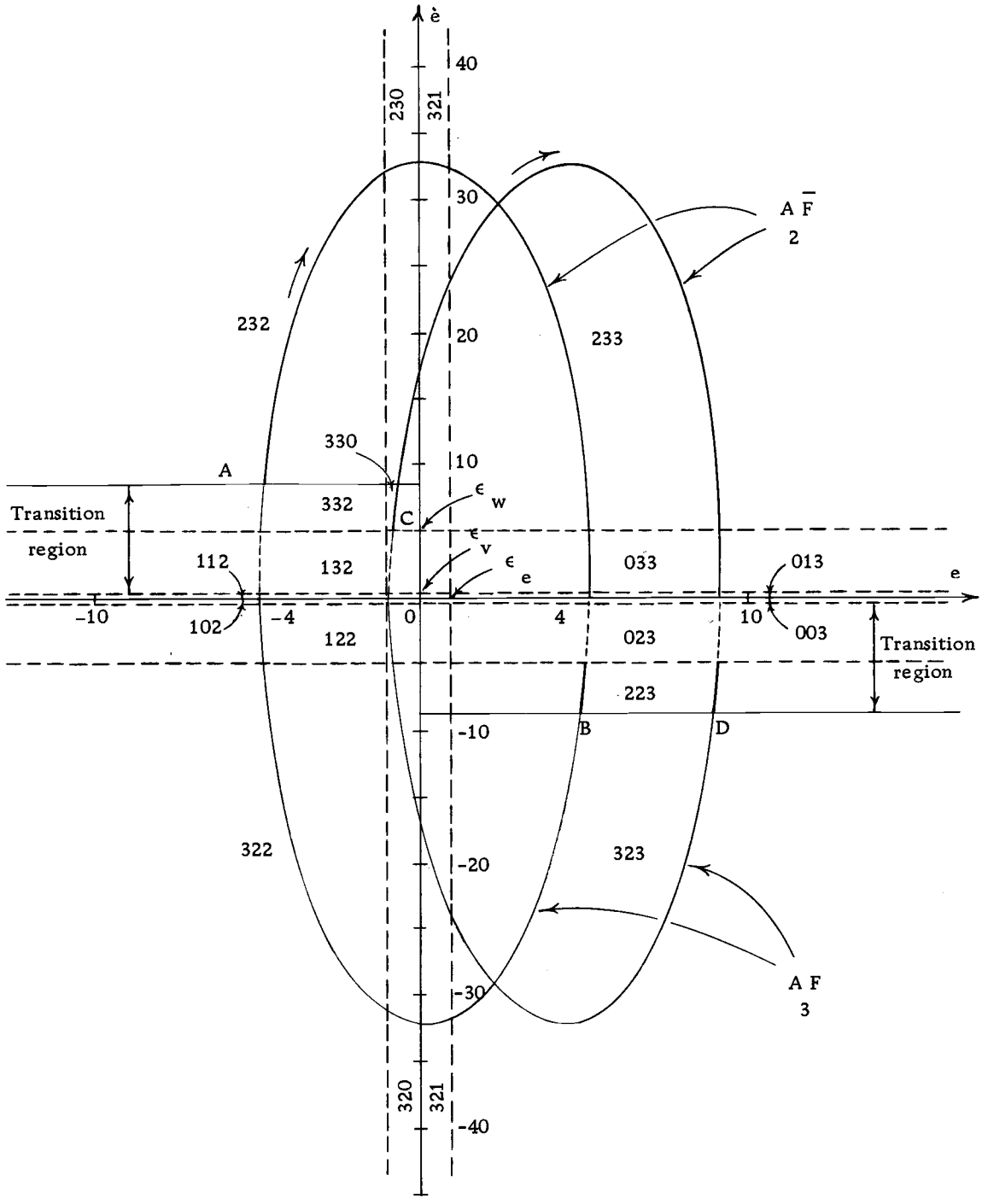

Figure 24. Typical phase plane patterns for the CNSS 3;CFLMS system. This figure shows that the average error may vary widely without changing the basic timing of the logic control signals which depend on the location of the state point. This allows the average error to drift between upper and lower limits. The "off-center" curve shows that the upper limit of this drift actually results from nonsymmetric timing. The lower limit arises similarly. At points A, B, and D switching is caused by table reversal. At point C, switching occurred before table reversal because of the control logic organization. (Compare with Figures 25, 10A, and 10B.)

illustrates how this logic pattern produced symmetric forward and reverse directed forces during each table cycle regardless of whether the average error for that cycle was positive or negative. (See also Figure 25.) This symmetry condition was possible only until the average error was approximately equal to the magnitude of an error cycle, at which time the state point passed near the origin and did not enter logic region 232, which introduced a nonsymmetry. Hence, the drift would proceed at a uniform rate until the average error became large enought to introduce such a nonsymmetry in the logic pattern which in turn reversed the direction of the drift.

Two criticisms of the CNSS 3 systems are that the dog showed no amplitude gain at any point and the asymptote seems to be at 20 dB/decade, neither of which are met by Figure 22. A general merit of the system is that it was quite insensitive to changes in the switching levels, especially for frequencies above the resonance. Increasing ϵ_w gradually changed the performance to be more like CNSS 2 systems, as would be expected. Decreasing ϵ_w caused little change until it approached the value of ϵ_v, at which time the drift became more pronounced. Change of α had effects similar to those for preceding systems except that the drift was greatly emphasized, nearly to the point of instability. The fast ramp response was essentially the same as for CNSS 2 systems.

Figure 26 is a gain-phase plot for the CNSS 3; VPLMS system.

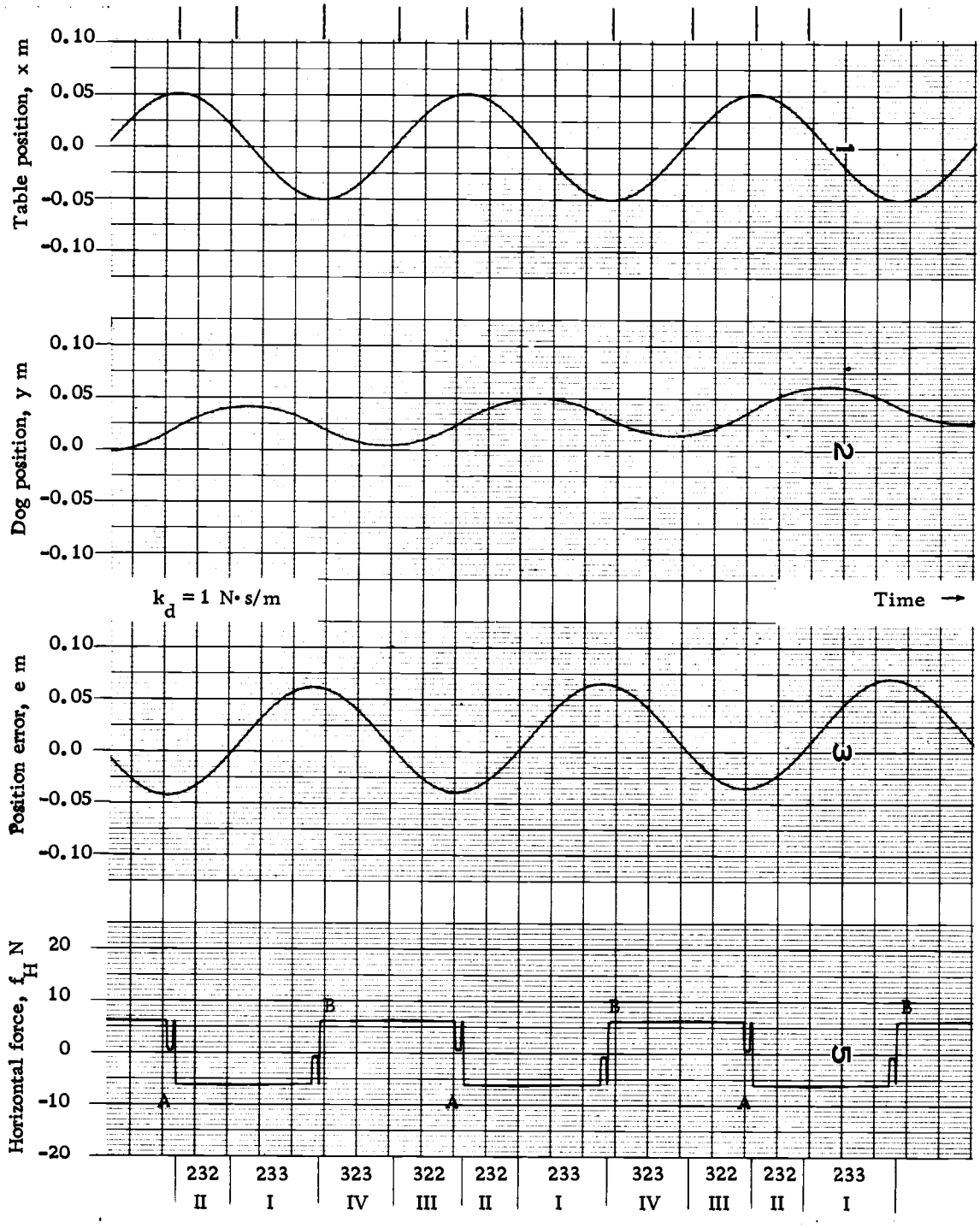

Figure 25. A typical display of three system variables with a sinusoidal input for the CNSS 3;CFLMS system. This figure shows the timing of the logic switching relative to the input for ω = 7 rad/s. The regions are marked to correspond with Figure 24, except that all of the transition regions are not shown. The transition regions appear as the notches. When the state point passes near the origin in Figure 24, the notch would be absent in one-half cycle, thus producing a nonsymmetry and reversing the drift. (Compare with Figure 24.)

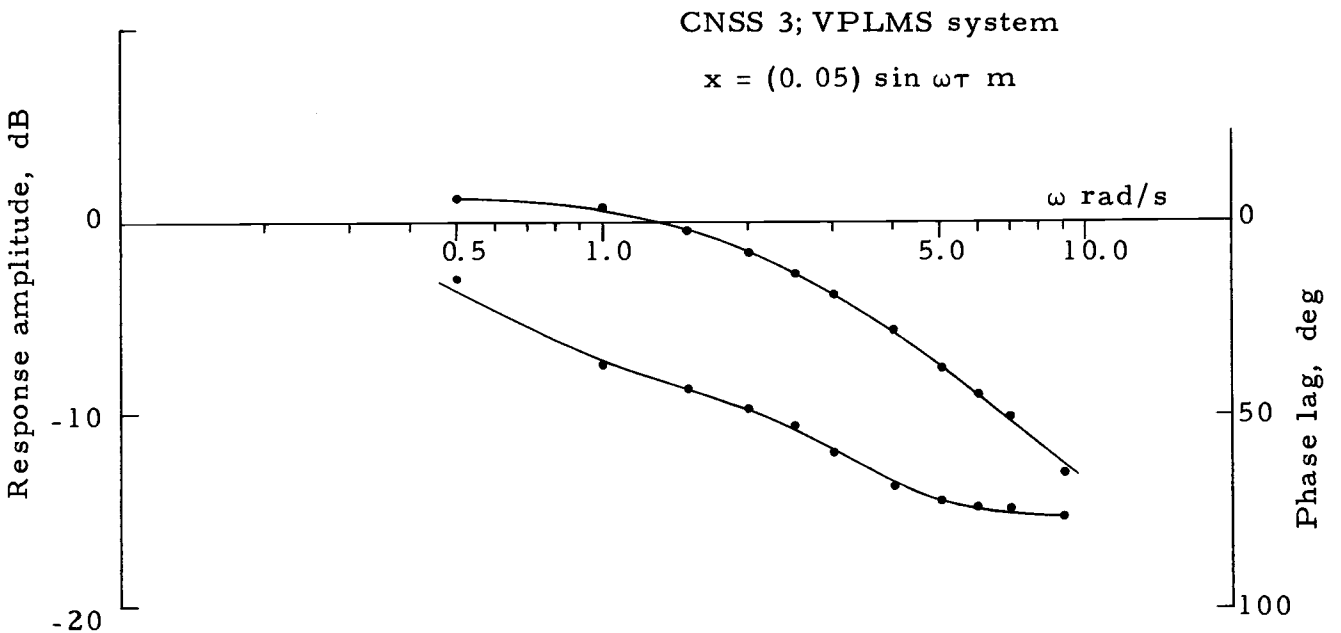

Figure 26. Amplitude and phase plot for the CNSS 3; VPLMS system. Comparison of this figure with Figure 12 shows there is a reasonable similarity between the behavior of this system and that of the dog.

The plot shows that this system very nearly agreed with the response data from the dog in both amplitude and phase. This suggested that velocity is a major control variable in the dog, both for controlling the horizontal force amplitude and the logic timing. (In previous CNSS 3 systems, the velocity was used only for logic timing.) Although the fast ramp response of this system showed undesired overshoot, by combining the constant-force and velocity-proportional muscle characteristics in an adaptive sense, characteristics very similar to the dog appear to be possible over a wide range of conditions.

Even though the system did not drift continuously as before, the average error was nonzero and an external force applied to the body was unopposed. When a combination of the constant-force and velocity-proportional muscles was simulated, as suggested above, the drift again appeared. For values of α unequal to 1, the CNSS 3; VPLMS system developed an unstable drift in the direction of application of the stronger force.

VI. EVALUATION OF WORK

One general impression gained from this work is that a systematic development of intuitive notions led to a model which, although crude, gave reasonable results in terms of the data obtained. Even at completion of this part of the UOMS experiment, enough new data were available to achieve a considerably more significant result by using the same method for developing the different systems.

Physiologically, the primary concern was to examine the major loop of the PCS known as the interoceptive loop, i.e., those parts of the PCS which respond to stimuli arising within the animal's own body. The extroceptive functions, i.e., those arising from stimuli external to the animal, were assumed to form a minor loop in the system and were neglected. The proprioceptive elements of the PCS, i.e., those responding to muscle tension or movement, were assumed to yield the joint angle of the legs continuously and precisely at all times.

The fact that the assumptions did not preclude development of a model showing characteristics which were reasonably compatable with observations suggests that the neglected functions are indeed secondary under the conditions of concern. A summary of the major assumptions is now given for review. 1) The legs and the backbone are rigid, massless members connected by pivots with viscous

friction and the body is a point mass. 2) Vertical accelerations and movements are negligible. 3) The head and neck are massless members. 4) The muscles act directly from nerve stimuli with no time delay. 5) All control is derived from either the joint angle, the rate of change of joint angle, or the table velocity, or some combination of these variables depending on the CNSS being considered. Accelerations are not considered in any case. 6) The state of the system may be described using no more than six Boolean logic variables with no time delays. 7) The volitional reference is time invariant.

Several of these assumptions bear further comment. First, consideration of vertical movements would lead to a separate control loop which would interact with the present major loop in some complex manner. The effects of vertical displacements would become more significant for larger table excursions or when the simulated condition is nearly to the point where the animal would fall over.

Second, the use of electronic logic to represent CNS functions was an oversimplification which carried only intuitive justification. At this stage, however, the assumption was nearly a necessity for work of this type. What effect a better simulation of the CNS functions might have is not known and will be the subject of further work.

Third, neglect of time delays was tolerated because the periodicity of the table movements would likely permit the PCS to make compensating predictions which would negate the effects of time

delays. An accurate simulation will need to separate the effects of prediction and time delay. At this level, however, it seemed reasonable to assume that the prediction compensated for time delays in such a way that attention can be limited to the prediction only. The use of nonperiodic table motion would require a reconsideration of this assumption. In a similar way, the nature of response in the muscle tissues would also become more significant whenever nonperiodic movements are studied.

Finally, the time invariant volitional reference has ignored all variations due to fatigue, "startle" effects, weight distributions, and external stimuli. These subjective factors would likely be more significant for nonperiodic movements and would also vary among different animals.

Regarding the extent of the data given, it should be fairly clear that this work was terminated for practical reasons, not because any part of it had really been completed. Considering the data available from the dog, it is not possible to evaluate the performance of the simulation model much further than has been done. Although more work could be done with the systems presented, the analysis of sinusoidal data is not expected to give a great deal more information than has been obtained. Realizing that the response to a sinusoidal table movement involves significant predictive and adaptive (learning) effects, nonperiodic and stochastic table movements will be needed for further

investigations to be useful. Since data of this type from the dog are lacking for the present, it is not possible to continue with such studies.

A substantial part of the UOMS experiment for the future will need to be devoted to studies designed to isolate the characteristics of each element within the PCS. An immediate problem in this regard arises from the observation that the interactions among the indifidual elements of the system tend to mask the details of these elements. As an example, the differences between the CFLMS and the TLMS were not nearly as clear when using CNSS 2 as when using CNSS 0, despite the significant differences between the two LMS's. Further, as previously explained, the effect of friction is nearly lost using CNSS 2 systems or with the CNSS 3; VPLMS system. Both the prediction and logic of the CNS may be expected to obscure significant system characteristics unless the experiments are very carefully designed to avoid this.

The work given here has dealt mostly with the PCS during smooth persuit operation. As in the case of the eye [5, 8], it is expected that different types of table movements will result in different system organization within the PCS. This amounts to saying that the PCS is capable of adapting to meet a variety of different disturbances in some optimal way. Hence, as different experiments are applied to an animal, it should be expected that the PCS organization will be

subject to significant changes. In the case of periodic table movement, one adaptation which appears likely would be for the animal to maintain balance (stability) while using minimum physical effort (energy).

Another observation supported by this work is that for systems whose control logic is significantly dependent on relative velocity, the "drift" characteristics originally observed in the dog are possible. The uncorrected error in average relative position is tolerated because the relative velocity rather than the relative position predominates in determining the timing of the force pattern.

Although it might be expected that a system change which altered the response amplitude curve would also alter the phase response curve to an equivalent extent, this idea was not really supported by the data. For example, the change from the CNSS 2; CFLMS system to the CNSS 3; CFLMS system altered the phase lags considerably without changing the response amplitude curves much at all. In studying the dog, it will be necessary to avoid confusion which could arise from this "nonuniqueness" characteristic of the PCS.

Another observation similar to those above is that regardless of the logic timing the amplitude plot retained its 40 dB/decade slope at higher frequencies. Although the timing changed the phase lag, the amplitude plot did not change significantly until a vastly different horizontal force from the LMS was employed (the VPLMS).

BIBLIOGRAPHY

1. Brookhart, J.M., P.L. Parmeggiani, W.A. Petersen and S.A. Stone. Postural stability in the dog. American Journal of Physiology 208:1047-1057. June 1965.

2. Brookhart, J.M., S. Mori and P.J. Reynolds. Digital afferent contributions to postural reactions. Portland, University of Oregon Medical School. (Abstract) Federation Proceedings 28:713. March-April 1969.

3. Brookhart, J.M. and W.A. Petersen. Unpublished research on postural stability in the dog, Project: Neurological study of postural control (NB-04744). Portland, University of Oregon Medical School, Department of Physiology. 1966.

4. Faber, J.J., G.R. Williamson and N.T. Feldman. Lubrication of joints. Journal of Applied Physiology 22:793-799. April 1967.

5. Fender, D.H. and P.W. Nye. An investigation of the mechanisms of eye movement control. Kybernetik 1:81-88. July 1961.

6. Lindgren, N. To understand brains. IEEE Spectrum 5:52-58. Sept. 1968.

7. Nakao, C. and J.M. Brookhart. Effects of labyrinthine and visual deprivation on postural stability. In: (Abstract) Proceedings of the fall meeting of the American Physiological Society, Howard University College of Medicine, August, 1967, Washington, D.C. The Physiologist 10:259. August 1967.

8. Robinson, D.A. The oculomotor control system: a review. Proceedings of the IEEE 56:1032-1049. June 1968.

APPENDICES

APPENDIX A

The Leg-Muscle Simulator

It is perhaps best to precede a description of the leg-muscle simulator (LMS) with an intuitive examination of the leg-muscle system which the LMS represents. We can begin by noting that the legs are simply a flexable coupling between the table and the dog's body and that all forces except gravity which act on the body must be transmitted through the legs, assuming that the animal is standing unaided. Further, if the resultant force on the body is resolved into its horizontal and vertical components, we see that the vertical component supports the body weight and the horizontal component produces horizontal acceleration which causes body motion. (Vertical accelerations were neglected since vertical motion seemed to be negligible for the short table excursions used in the UOMS experiment.)

The magnitude of the horizontal force transmitted through the legs is a function of both the muscle tension and the leg position. This must be the case or the dog could not control his position. It is quite easy to see that the muscle tension controls the stiffness of the legs, and hence, has a direct effect on the magnitude of the horizontal force applied to the body. We will see later, however, that the muscle tension may actually be separated into two parts, one of which supports the body while the other accelerates the body horizontally.

It remains now to consider how leg position can also effect the horizontal force magnitude. This may be illustrated by recalling how it is possible to increase horizontal force capability by leaning into a load. The leaning action allows the axial force transmitted through the legs to have a component directed horizontally which will increase as the angle of the leg increases.

With this background, we can now give attention to the development of the LMS. According to the model of the dog's body given in Chapter II, the legs were simply rigid, massless levers which were pivoted at the body (hip or shoulder joints) and could be activated by the muscles. Further, since skidding of the feet was neglected, the foot of each leg was assumed equivalent to a free pivot at the table surface. The mechanical model resulting from these assumptions was used as the basis for the LMS. A "one-leg" representation of this model appears in Figure A-1. (The one leg represents the combined effects of all four legs. Since the four legs were taken to be identical, vertical accelerations were neglected, and the body was reduced to an equivalent point mass, the one conceptual leg is exactly equivalent to four separate legs.) The lever is analogous to the leg bones while the total musculature of the four legs is represented by the muscle simulator.

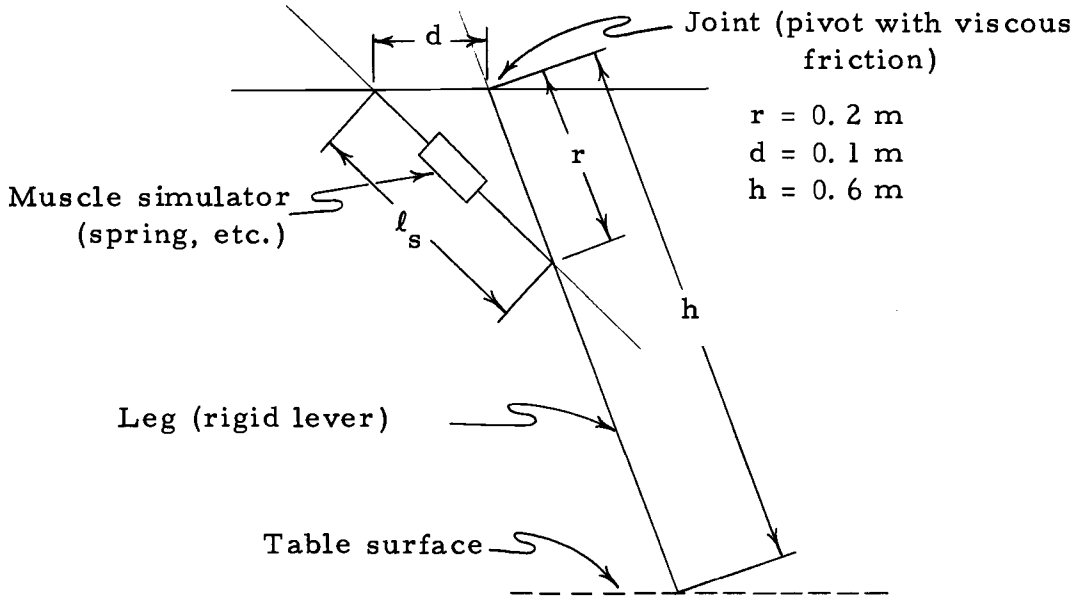

Figure A-1. The model used for the LMS. This model is a result of the assumptions discussed in Chapter II. The mechanical form of the model was the same for each LMS. The different muscle characteristics were obtained by allowing the muscle simulator to be described by four different conceptual tension functions.

The function of the LMS was to generate a horizontal force which was a function of leg position (joint angle) and muscle tension, where the muscle tension was in turn a function of leg position (or relative velocity for the VPLMS) and the binary control variables A and F. The functional form for the horizontal force f_H appears as Equation (A-1), where $g(|\theta|, A, F)$, as seen in

$$f_H = f[g(|\theta|, A, F), |\theta|], \qquad (A-1)$$

is the tension of the muscle simulator. We now proceed to reduce

the function $f[g(|\theta|,A,F),|\theta|]$ as follows:

$$\begin{aligned} f_H &= f[g(|\theta|),|\theta|] && \text{A-true, F-true} \\ &= -\frac{1}{\alpha} f[g(|\theta|),|\theta|] && \text{A-true, F-false} \\ &= \frac{1}{\beta} f[g(|\theta|),|\theta|] && \text{A-false, F-true} \\ &= -\frac{1}{\alpha\beta} f[g(|\theta|),|\theta|] && \text{A-false, F-false .} \end{aligned} \tag{A-2}$$

Observing this set of equations, we see that the multiplicative scale factors $1/\alpha$ and $1/\beta$ have been applied to the total force function f rather than to the muscle tension function g. Actually, for the computer simulator to correspond directly to the mechanical model of Figure A-1, these scale factors should have been applied to the muscle tension function g. However, since the resulting force generated would have been the same for either case, the above form was chosen for its convenience in the simulation. Mathematically, this choice is possible because

$$f[g(|\theta|,A,F,),|\theta|] = f[g(|\theta|),|\theta|,A,F,]$$

and

$$f[\{\frac{1}{\alpha}g(|\theta|)\}] = \frac{1}{\alpha} f[g(|\theta|),|\theta|].$$

To obtain the output function shown by Equations (A-2), the LMS was subdivided into two sections. One section generated

$f[g(|\theta), |\theta|]$, which represented the combined effects of the legs and muscles. Following this section, the magnitude scaling and sign control was achieved with a network of potentiometers, electronic switches, and amplifiers, where the switches were activated by the control variables A and F. We will shortly consider each of these sections of the simulator; however, before the first section can be treated, it is necessary to present a characteristic of the muscle tension in animals which will be used to describe the function $f[g(|\theta|), |\theta|]$.

Physiologists have traditionally divided muscle tissue into two types--phasic and tonic. The phasic tissue is thought to produce forces of a dynamic nature such as are required for rapid movements. The tonic tissue appears to provide the muscle tone which is required to support static loads. Hence, the force from the muscle simulator was designated to be the sum of two forces, as expressed in Equation (A-3). The magnitude of T_{ton} was limited by

$$g(|\theta|) = T_{ph}(|\theta|) + T_{ton}(|\theta|) \qquad \text{(A-3)}$$

to be such that it exactly supported the body weight while the magnitude function for T_{ph} was allowed to be one of several forms which seemed meaningful. Choices for T_{ph} will be discussed later.

Returning to the development of section one of the LMS which generated the function $f[g(|\theta|), |\theta|]$, recall that this function was

designed to represent the characteristics of the level model of Figure A-1. From the free body diagram of Figure A-2, we can derive the functional relation between the horizontal force f_H (coupled from the table to the body through the legs) and the tension in the muscle simulator.

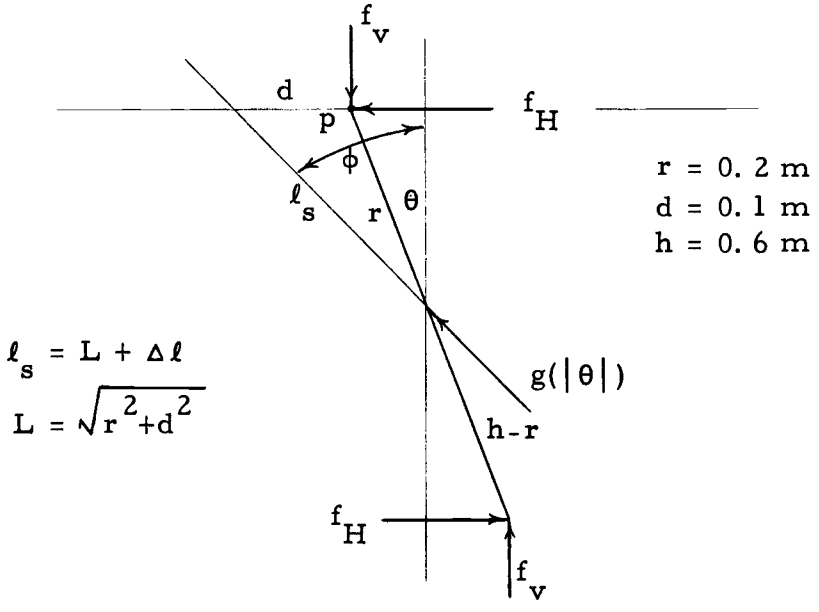

Figure A-2. A free body diagram for the leg-muscle model of Figure A-1. The functional form of the horizontal force function f was obtained from this diagram by the methods of static mechanics.

To obtain an equation describing the relation between f_H and g when both A and F are true, consider the free body diagram given in Figure A-2. Conveniently, the principles of statics may be applied since the leg member was assumed to be massless. The equation needed to relate f_H and $g(|\theta|)$, thus giving the form of the function f, was obtained by summing moments about the

pivot P, $\sum M_p = 0$ (clockwise). This gave

$$-f_H h \cos\theta - f_V h \sin\theta + g(|\theta|) r \sin(\phi-\theta) = 0 . \qquad (A-4)$$

Solving Equation (A-4) for f_H, the result is

$$f_H = \frac{rdg(|\theta|)}{h\ell_s} - \frac{hf_V|y-x|}{h^2} = \frac{rdT_{ph}(|\theta|)}{h\ell_s} + \left[\frac{rdT_{ton}(|\theta|)}{h\ell_s} - \frac{hf_V|y-x|}{h^2}\right], \qquad (A-5)$$

where

$$\cos\theta \doteq 1, \quad \sin\theta = |y-x|/h, \quad \sin(\phi-\theta) \doteq d/\ell_s .$$

In Equation (A-5), T_{ton} was chosen so that the term in the parentheses became identically zero for all values of θ. This determined the form of the f function to be

$$f[g(|\theta|), |\theta|] = f[T_{ph}(|\theta|), |\theta|] = \frac{rdT_{ph}(|\theta|)}{h\ell_s} . \qquad (A-6)$$

Several different forms were chosen for T_{ph} so that the effects of considerably different muscle characteristics could be compared. Specifically, T_{ph} was chosen to represent one of the following four muscle types: 1) a torsional spring at the pivot (TLMS), 2) a linear spring as the muscle simulator (SLMS), 3) a constant force device as the muscle simulator (CFLMS), or 4) a velocity-proportional muscle simulator (VPLMS). In the last case, note that

T_{ph} is a function of $|\dot{\theta}|$ rather than $|\theta|$, since $|\dot{\theta}| \doteq |\dot{y}-\dot{x}|/h$. The equations for these four cases are given below in respective order.

$$f[g(|\theta|), |\theta|] = \frac{rd}{h\ell_s}\left(\frac{\ell_s}{rd} k_t |\theta|\right) \quad \text{TLMS} \qquad \text{(A-7)}$$

$$= \frac{rd}{h\ell_s}(k_s \Delta\ell) \quad \text{SLMS} \qquad \text{(A-8)}$$

$$= \frac{rd}{h\ell_s}(k_{cf}) \quad \text{CFLMS} \qquad \text{(A-9)}$$

$$= \frac{rd}{h\ell_s}[k_{vp}|\dot{y}-\dot{x}|] \quad \text{VPLMS} \qquad \text{(A-10)}$$

We now proceed to reduce each of these equations to show how the different forms of the f function were generated. First, consider the TLMS of Equation (A-7). We can simplify by substitution as follows:

$$\frac{rd}{h\ell_s}\left(\frac{\ell_s}{rd} k_t |\theta|\right) = \frac{k_t}{h}\frac{|y-x|}{h} \qquad \text{(A-11)}$$

where

$$\theta \doteq \sin\theta = |y-x|/h \,.$$

Clearly, we have that

$$f[g(|\theta|), |\theta|] = \frac{k_t}{h^2}|y-x| \,, \qquad \text{(A-12)}$$

which is simply a constant times the error magnitude. The computer

configuration for this generator used only a potentiometer for scaling and is not explicitly shown here.

Second, the SLMS of Equation (A-8) was reduced as follows:

$$\frac{rd}{h\ell_s}(k_s \Delta\ell) = \frac{rdk_s}{h}\left(\frac{\Delta\ell}{L+\Delta\ell}\right). \tag{A-13}$$

The only variable term in this equation is $\Delta\ell/(L+\Delta\ell)$, which is a function of the angle θ. The following equations show how this term was reduced for computer generation.

Let $d = \eta r$ where $\eta > 0$, and $\theta \doteq \sin\theta = \frac{|y-x|}{h}$. Then

$$L = [r^2+d^2]^{1/2} = r[1+\eta^2]^{1/2}. \tag{A-14}$$

By the law of consines,

$$\ell_s = (L+\Delta\ell) = [r^2+d^2-2rd\cos(90+\theta)]^{1/2}. \tag{A-15}$$

Simplifying,

$$\begin{aligned}(L+\Delta\ell) &= [r^2+\eta^2r^2+2r\eta r\sin\theta]^{1/2} \\ &= r\left[1+\eta^2+2\eta\frac{|y-x|}{h}\right]^{1/2}.\end{aligned} \tag{A-16}$$

We can now obtain $\Delta\ell$ from the identity

$$\Delta\ell = (L+\Delta\ell) - L. \tag{A-17}$$

Figure A-3 shows how these functions were generated on the analog

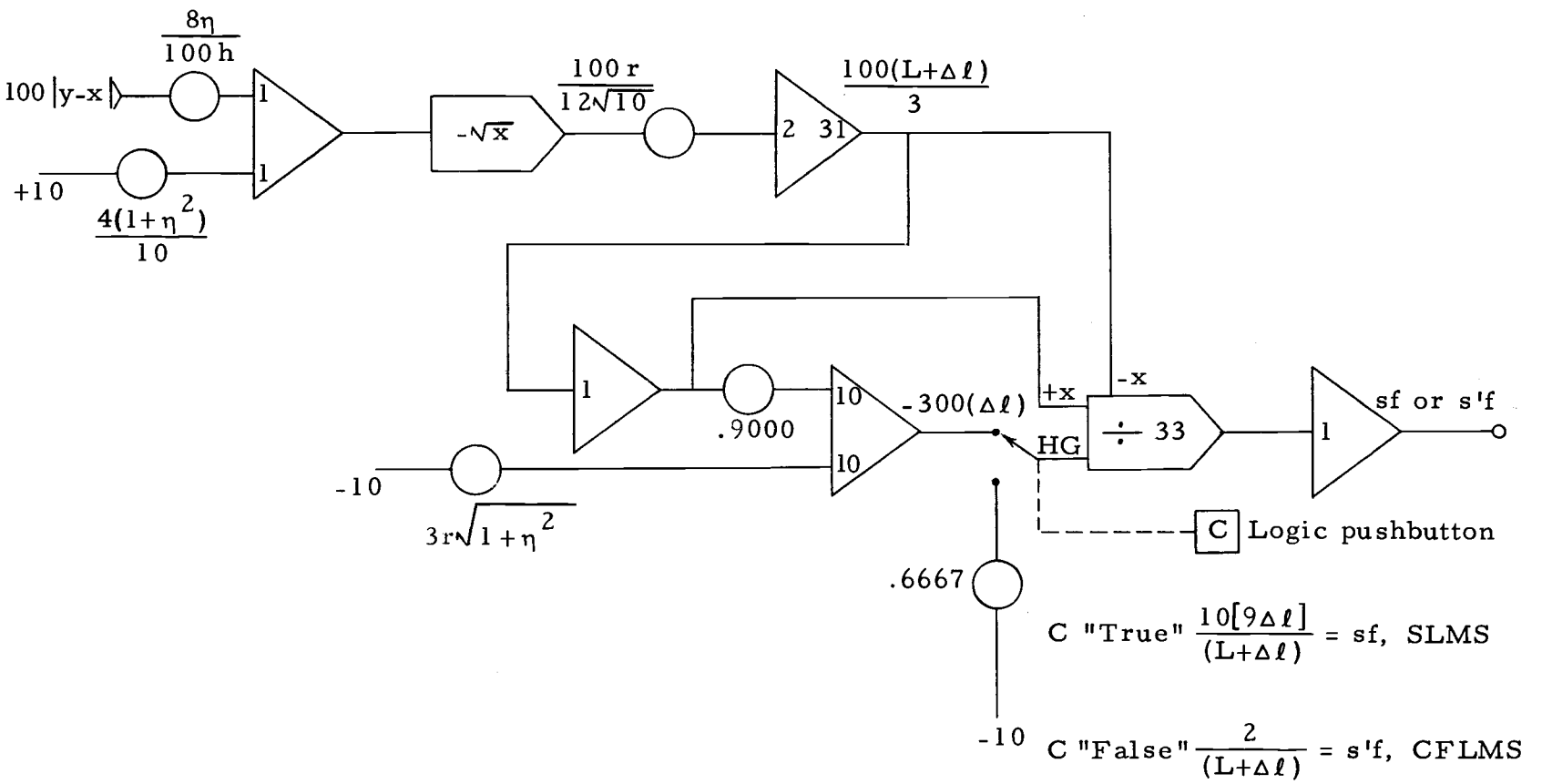

Figure A-3. The logic-analog computer diagram of the LMS function generator. This is the first section of the LMS which generated the horizontal force function f (scaled) that was an input to the second section of the LMS.

computer.

Third, Equation (A-9) assumed that the tension $T_{ph}(\theta)$ was a constant, k_{cf}. This equation reduced as follows:

$$\frac{rd}{h\ell_s}(k_{cf}) = \frac{rdk_{cf}}{h}\left(\frac{1}{L+\Delta\ell}\right) . \qquad (A-18)$$

To generate this function, it was simply required to obtain the scaled inverse of the output of amplifier 31 in Figure A-3, which is equal to $100\,(L+\Delta\ell)/3$. This was accomplished by applying a constant voltage to the HG input of the divider 33, thus obtaining $2/(L+\Delta\ell)$.

Fourth, Equation (A-10) was revised as shown by Equation (A-19) below.

$$\frac{rd}{h\ell_s}(k_{vp}|\dot{y}-\dot{x}|) = \frac{rdk_{vp}}{h}\left(\frac{|\dot{y}-\dot{x}|}{L+\Delta\ell}\right) \qquad (A-19)$$

This function was generated by applying the scaled relative velocity signal to the HG input of divider 33. The output of the divider became $k'|\dot{y} - \dot{x}|/(L+\Delta\ell)$ which represented a force of 6N for a leg angle of 5 deg and a relative velocity of 0.097 m/s.

At this point, we summarize the preceding developments. First,

$$f[g(|\theta|), |\theta|] = \frac{rd}{h\ell_s} T_{ph}(|\theta|) . \qquad (A-6)$$

The reduced forms of this equation for the four different muscle types are repeated below.

$$f[g(|\theta|), |\theta|] = \frac{k_t}{h^2} |y-x| \qquad \text{TLMS} \qquad \text{(A-12)}$$

$$= \frac{rdk_s}{h} \left(\frac{\Delta \ell}{L+\Delta \ell}\right) \qquad \text{SLMS} \qquad \text{(A-13)}$$

$$= \frac{rdk_{cf}}{h} \left(\frac{1}{L+\Delta \ell}\right) \qquad \text{CFLMS} \qquad \text{(A-18)}$$

$$= \frac{rdk_{vp}}{h} \left(\frac{|\dot{y}-\dot{x}|}{L+\Delta \ell}\right) \qquad \text{VPLMS} \qquad \text{(A-19)}$$

Having obtained the function $f[g(|\theta|), |\theta|]$, the second section of the LMS can be presented. This stage received the above analog function (scaled) and the control variables A and F as inputs and generated f_H (scaled) as its output. The computer diagram which was used is given in Figure A-4. The electronic switches shown were standard components on the EAI 680 computer. The switches were closed whenever the corresponding logic variables were true.

Since the computer used for this work contained less than one quarter of the full component schedule, this section of the LMS was not implemented on the machine exactly as shown. However, the configuration used gave the same result as could have been gained with the following diagram. This diagram is given since it is more readily understood than the actual one used.

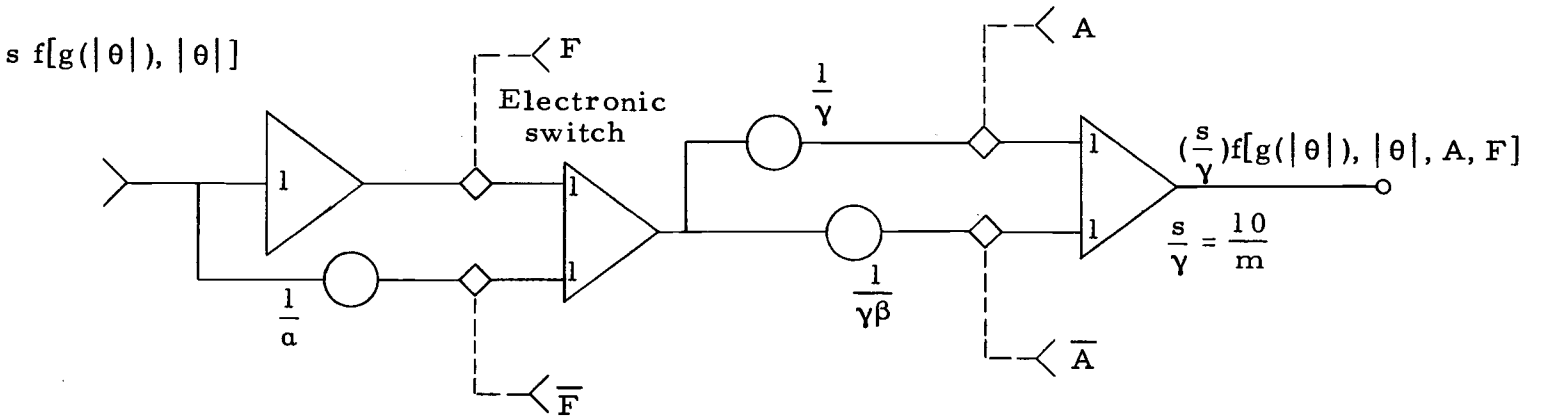

Figure A-4. The logic-analog computer diagram of the second section of the LMS. This diagram shows how the horizontal force function f was amplitude scaled or negated according to the logic control variables A and F from the CNSS.

APPENDIX B

Design of Logic Systems

The logic systems for the response integration simulator (RIS) were formulated using the elementary procedures of Boolean logic reduction followed by AND-gate synthesis. It is assumed that the reader is slightly familiar with the basic Boolean postulates and the use of Karnaugh maps for logic reduction.

For each system, the truth table is the same as was presented in Chapter II and is repeated here for convenience. The logical expressions for the RIS output variables have been obtained in reduced form from Karnaugh maps and the logical functions are written in suitable form for AND-gate synthesis.

Observing Table B-1, we see that RIS 0 was an obviously degenerate case where A was always "true" and $F = \overline{P}$. The input variables not shown were permitted in any combination of logical states without affecting the output variables. The simplicity of this system allowed it to be realized without use of any logical gates.

The second system, RIS 1, is given in Table B-2. The logical expressions derived from the Karnaugh maps in Figure B-1 were also realized without using any logical gates.

Table B-1. RIS 0 truth table.

Input condition		Output condition	
$\overline{P}$	0	A F	3
P	1	A $\overline{F}$	2

Table B-2. RIS 1 truth table.

Input condition		Output condition	
$\overline{E}\,\overline{P}$	0	$\overline{A}$ F	1
$\overline{E}$ P	1	$\overline{A}\,\overline{F}$	0
E $\overline{P}$	2	A F	3
E P	3	A $\overline{F}$	2

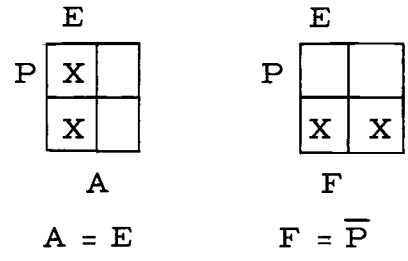

Figure B-1. RIS 1 Karnaugh maps. The Karnaugh maps in this figure were derived from Table B-2. The resulting logical functions were used for RIS 1.

The logical expressions for RIS 2 were more involved, as can be guessed by observing Table B-3. The four-variable Karnaugh maps given in Figure B-2 were written to obtain expressions for the inverses of both A and F. This permitted the system to be synthesized using fewer gates than would have been needed otherwise.

The first equation in the figure gives the logical expression using both the AND and OR notation while the second expressions have been reduced to the AND-gate form using De Morgan's theorem, i. e., $\overline{A + B} = \overline{A}\,\overline{B}$ or $A + B = \overline{\overline{A}\,\overline{B}}$.

Table B-3. RIS 2 truth table.

Input condition		Output condition	
$\overline{V}\,\overline{S}\,\overline{E}\,\overline{P}$	00	$\overline{A}\,F$	1
$\overline{V}\,\overline{S}\,\overline{E}\,P$	01	$\overline{A}\,\overline{F}$	0
$\overline{V}\,\overline{S}\,E\,P$	02	$A\,F$	3
$\overline{V}\,\overline{S}\,E\,P$	03	$A\,\overline{F}$	2
$\overline{V}\,S\,\overline{E}\,\overline{P}$	10	$\overline{A}\,F$	1
$\overline{V}\,S\,\overline{E}\,P$	11	$\overline{A}\,\overline{F}$	0
$\overline{V}\,S\,E\,\overline{P}$	12	$A\,F$	3
$\overline{V}\,S\,E\,P$	13	$A\,\overline{F}$	2
$V\,\overline{S}\,\overline{E}\,\overline{P}$	20	$A\,F$	3
$V\,\overline{S}\,\overline{E}\,P$	21	$A\,F$	3
$V\,\overline{S}\,E\,\overline{P}$	22	$A\,F$	3
$V\,\overline{S}\,E\,P$	23	$\overline{A}\,\overline{F}$	0
$V\,S\,\overline{E}\,\overline{P}$	30	$A\,\overline{F}$	2
$V\,S\,\overline{E}\,P$	31	$A\,\overline{F}$	2
$V\,S\,E\,\overline{P}$	32	$\overline{A}\,F$	1
$V\,S\,E\,P$	33	$A\,\overline{F}$	2

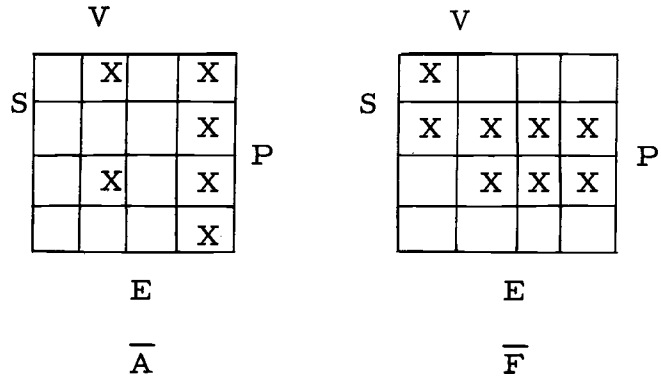

$$\overline{A} = \overline{V}\,\overline{E} + V\,S\,E\,\overline{P} + V\,\overline{S}\,E\,P$$

$$A = (\overline{\overline{V}\,\overline{E}} \cdot \overline{V\,S\,E\,\overline{P}} \cdot \overline{V\,\overline{S}\,E\,P})$$

$$\overline{F} = E\,P + \overline{V}\,P + V\,S\,\overline{E}$$

$$F = (\overline{E\,P} \cdot \overline{\overline{V}\,P} \cdot \overline{V\,S\,\overline{E}})$$

Figure B-2. RIS 2 Karnaugh maps. These Karnaugh maps were derived from Table B-3 and provided the logical functions for RIS 2 in reduced form.

The final system, RIS 3, is described by Table B-4. The truth table shows only those combinations of the input variables which could physically occur. (When V is "false", W must also be "false", hence, it is not possible to have a condition such as W X $\overline{V}$ S E P, etc.) Because RIS 3 and RIS 2 were quite similar, it seemed less complicated to synthesize RIS 3 by adding a logical modification to RIS 2, rather than to construct a new system of logic. Hence, the equations for RIS 3 were written intuitively by observing the differences between RIS 2 and RIS3. Defining A' and F' to be the desired outputs for RIS 3, logical expressions for these variables were obtained in terms

Table B-4. RIS 3 truth table.

Input condition		Output condition	
$\overline{W}\ \overline{X}\ \overline{V}\ S\ \overline{E}\ \overline{P}$	000	$\overline{A}$ F	1
⋮ Same as RIS 2		⋮	
$\overline{W}$ X V S E P	133	A $\overline{F}$	2
W $\overline{X}\ \overline{V}\ S\ \overline{E}\ \overline{P}$	200	...	
⋮ Not physically possible, $\overline{V} \rightarrow \overline{W}$			
W $\overline{X}\ \overline{V}$ S E P	213	...	
W $\overline{X}$ V $\overline{S}\ \overline{E}\ \overline{P}$	220	A F	3
W $\overline{X}$ V $\overline{S}\ \overline{E}$ P	221	A F	3
W $\overline{X}$ V $\overline{S}$ E $\overline{P}$	222	A F	3
W $\overline{X}$ V $\overline{S}$ E P	223	A $\overline{F}$	2
W $\overline{X}$ V S $\overline{E}\ \overline{P}$	230	A $\overline{F}$	2
W $\overline{X}$ V S $\overline{E}$ P	231	A $\overline{F}$	2
W $\overline{X}$ V S E $\overline{P}$	232	A $\overline{F}$	2
W $\overline{X}$ V S E P	233	A $\overline{F}$	2
W X $\overline{V}\ \overline{S}\ \overline{E}\ \overline{P}$	300	...	
⋮ Not physically possible, $\overline{V} \rightarrow \overline{W}$			
W X $\overline{V}$ S E P	313	...	
W X V $\overline{S}\ \overline{E}\ \overline{P}$	320	A F	3
W X V $\overline{S}\ \overline{E}$ P	321	A F	3
W X V $\overline{S}$ E $\overline{P}$	322	A F	3
W X V $\overline{S}$ E P	323	A F	3
W X V S $\overline{E}\ \overline{P}$	330	A $\overline{F}$	2
W X V S $\overline{E}$ P	331	A $\overline{F}$	2
W X V S E $\overline{P}$	332	A F	3
W X V S E P	333	A $\overline{F}$	2

of W, X, A, F, and combinations of V S E P, where A and F were the outputs from RIS 2. Thexe expressions are

$$A' = \overline{W}\,A + W$$
$$\overline{A}' = (\overline{\overline{W}\,A} \cdot \overline{W}) \tag{B-1}$$

and

$$F' = \overline{W}\,F + W\,X\,(V\,\overline{S}\,E\,P + V\,S\,E\,\overline{P}) + W\,F\,\overline{S}$$
$$\overline{F}' = \overline{W}\,F \cdot \overline{[\overline{W\,X} \cdot \overline{(V\,\overline{S}\,E\,P} \cdot \overline{V\,S\,E\,\overline{P})}]} \cdot \overline{W\,F\,\overline{S}}\,. \tag{B-2}$$

Although synthesis by this method was likely not optimal in terms of the number of logical gates used, it required less additional logic than would have been needed to form a new simulator system that was independent of RIS 2.

Due to the limited availability of logic on the EAI 680 logic-analog computer at the time of this work, Motorola integrated circuit logic elements of the MECL type (MC 350 series) were used. With this type of logic, only NOR-gates were available, hence, all logical expressions were converted to the NOR-gate form rather than the form given here, by using De Morgan's theorem. It was also necessary to convert the logic levels through an interface with the computer since the EAI 680 used levels of 0 and 5 V while the MECL logic levels were -1.5 and -0.75 V, respectively.

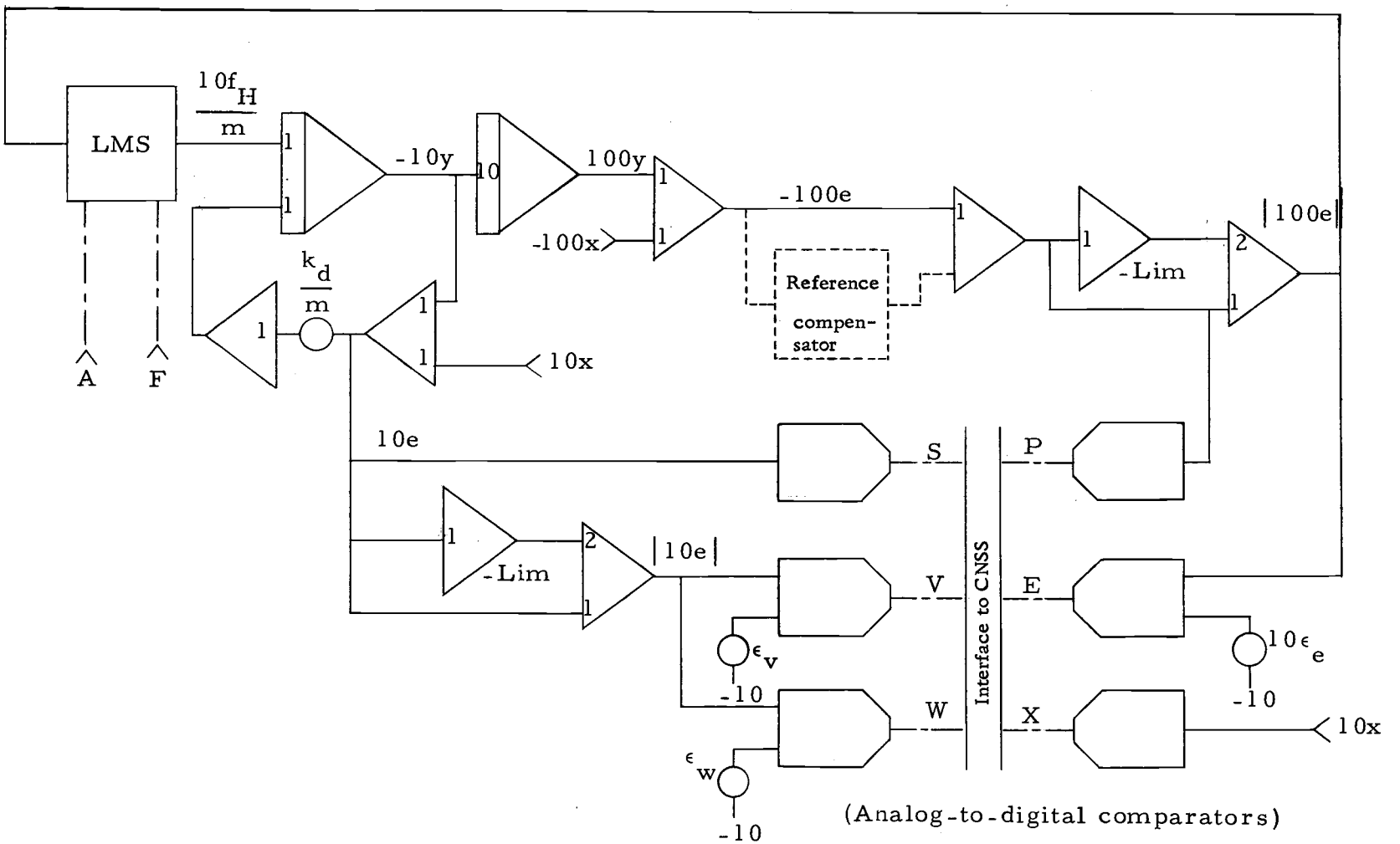

Figure C-1. The basic simulation diagram. This diagram shows the arrangement of the logic-analog computer elements as they were used. Note that the LMS is shown as a block and only the logic interface with the CNSS appears here.